NASA TECHNICAL MEMORANDUM

NASA TM X-73,082

NASA TM X-73,082

IMPLICIT APPROXIMATE-FACTORIZATION SCHEMES FOR THE LOW-FREQUENCY TRANSONIC EQUATION

William F. Ballhaus and Joseph L. Steger

Ames Research Center
and
U.S. Army Air Mobility R & D Laboratory
Moffett Field, California 94035

November 1975

1 Report No.	2. Government Accession No.	3. Recipient's Catalog No.
TM X-73,082		

4. Title and Subtitle	5. Report Date
IMPLICIT APPROXIMATE-FACTORIZATION SCHEMES FOR THE LOW-FREQUENCY TRANSONIC EQUATION	6. Performing Organization Code

7. Author(s)	8. Performing Organization Report No.
William F. Ballhaus and Joseph L. Steger	A-6373

9. Performing Organization Name and Address	10. Work Unit No.
Ames Research Center and U.S. Army Air Mobility R & D Laboratory Moffett Field, California 94035	11. Contract or Grant No.

12. Sponsoring Agency Name and Address	13. Type of Report and Period Covered
National Aeronautics and Space Administration Washington, D. C. 20546	Technical Memorandum
	14 Sponsoring Agency Code

15. Supplementary Notes

16. Abstract

Two- and three-level implicit finite-difference algorithms for the low-frequency transonic small disturbance-equation are constructed using approximate factorization techniques. The schemes are unconditionally stable for the model linear problem. For nonlinear mixed flows, the schemes maintain stability by the use of conservatively switched difference operators for which stability is maintained only if shock propagation is restricted to be less than one spatial grid point per time step. The shock-capturing properties of the schemes are studied for various shock motions that might be encountered in problems of engineering interest. Computed results for a model airfoil problem that produces a flow field similar to that about a helicopter rotor in forward flight show the development of a shock wave and its subsequent propagation upstream off the front of the airfoil.

17. Key Words (Suggested by Author(s))	18. Distribution Statement
Unsteady transonic flow Implicit finite difference schemes	Unlimited STAR Category — 64

19. Security Classif. (of this report)	20. Security Classif. (of this page)	21. No. of Pages	22. Price*
Unclassified	Unclassified	43	$3.75

*For sale by the National Technical Information Service, Springfield, Virginia 22151

IMPLICIT APPROXIMATE-FACTORIZATION SCHEMES FOR THE LOW-FREQUENCY TRANSONIC EQUATION

William F. Ballhaus and Joseph L. Steger

Ames Research Center
and
U.S. Army Air Mobility R&D Laboratory
Moffett Field, California 94035

SUMMARY

Two- and three-level implicit finite-difference algorithms for the low-frequency transonic small disturbance-equation are constructed using approximate factorization techniques. The schemes are unconditionally stable for the model linear problem. For nonlinear mixed flows, the schemes maintain stability by the use of conservatively switched difference operators for which stability is maintained only if shock propagation is restricted to be less than one spatial grid point per time step. The shock-capturing properties of the schemes are studied for various shock motions that might be encountered in problems of engineering interest. Computed results for a model airfoil problem that produces a flow field similar to that about a helicopter rotor in forward flight show the development of a shock wave and its subsequent propagation upstream off the front of the airfoil.

I. INTRODUCTION

Frequently, one employs simplified equations that extract the essential physics from a more complete set of equations that model some physical phenomenon. These simplifications, while limiting the range of applicability, often significantly reduce the complexity and expense of computing solutions. When such approximations are made, the numerical algorithm used to solve the simplified equations should be matched to the same range of applicability.

Of interest here is the solution of the transonic flow field about a thin airfoil executing some arbitrary small amplitude oscillatory motion in a uniform stream. The small disturbance and transonic assumptions allow simplification of the governing gas-dynamic equations to (ref. 1, p. 4)

$$k^2 M_\infty^2 \phi_{tt} + 2kM_\infty^2 \phi_{xt} = V_c \phi_{xx} + \phi_{yy} \tag{1}$$

where $V_c = 1 - M_\infty^2 - (\gamma + 1) M_\infty^m \phi_x$, ϕ is the disturbance velocity potential, γ is the ratio of specific heats, and m is a function of M_∞ (see refs. 2 and 3). The coordinate system is fixed with respect to the airfoil, and x is alined with the free-stream direction. The flow is defined to be locally subsonic or supersonic, relative to the fixed coordinate system, for $V_c > 0$ or $V_c < 0$, respectively. A measure of the degree of unsteadiness of the motion is given by the reduced frequency k; for an airfoil of chord length ℓ, with free-stream velocity U_∞, and executing some periodic motion of frequency ω,

$$k = \frac{\omega c}{U_\infty} \tag{2}$$

The variables ϕ, t, y, and x have been nondimensionalized by cU_∞, $1/\omega$, c, and c, respectively. In the derivation of (1), it is assumed that the flow is inviscid and transonic ($M_\infty \approx 1$) and that velocity disturbances due to the airfoil are small compared to U_∞. Further simplification can be achieved by restricting the range of reduced frequencies, as we shall see.

The traces of the characteristic surfaces in the plane of the airfoil for the linear form of (1) are shown in figure 1. Waves that *advance* in the flow direction propagate downstream relative to the airfoil with velocity $(M_\infty + 1)/M_\infty k$ in the nondimensional coordinate system. Waves that *recede* (relative to particle paths) travel upstream against the flow with velocity $(M_\infty - 1)/M_\infty k$. Fluid particles travel with velocity $1/k$ (i.e., U_∞ in the dimensional system). For low-frequency transonic flows (ref. 4),

$$k \sim 1 - M_\infty^2 \sim \tau^{2/3} << 1 \tag{3}$$

where τ is the airfoil thickness-to-chord ratio. So disturbances traveling along the advancing waves propagate rapidly away from the airfoil, while those traveling along the receding waves remain closer to the airfoil and dominate the solution there. For low-frequency motion, (1) reduces to the low-frequency, transonic, small-disturbance equation

$$2kM_\infty^2\phi_{xt} = V_c\phi_{xx} + \phi_{yy} \tag{4}$$

which is subject to the restrictions (3). The numerical solution of (4) is useful, for example, in aerodynamic flutter analysis and the treatment of high speed helicopter rotors.

An efficient computational algorithm for either (1) or (4) should have a time step restriction for stability that is no more restrictive than the time step required to adequately resolve the unsteady flow field. Since, for low-frequency motions, the solution is dominated by disturbances traveling along the receding waves, the time step should be related to the time scale of receding wave propagation, as well as the wave length of these disturbances. Explicit schemes for transonic flows have time step restrictions for stability that are based on the advancing wave time scale. Hence, for low-frequency motion, they have time step restrictions for stability that can be orders of magnitude more severe than required for accuracy. This problem of stiffness was overcome in reference 4 by the use of semi-implicit difference schemes applied to (1) and (4), with a resulting time step restriction based solely on the receding wave time scale.

Results obtained using the semi-implicit scheme applied to (4) have been compared with solutions to the complete Eulerian gas-dynamic equations in references 2 and 3. The solutions compared favorably for cases in which the assumptions (3) were valid, and the simplified theory resulted in a considerable savings in computer run time and storage. However, it will be shown in what follows that considerably larger time steps than allowed by the semi-implicit scheme stability requirement

$$\Delta t \leq \frac{2kM_\infty{}^2\Delta x}{|1 - M_\infty{}^2 - (\gamma + 1)M_\infty{}^m\phi_x|} \tag{5}$$

can be taken without sacrificing accuracy for truly low-frequency motions. Note that (5) is especially restrictive near the airfoil leading and trailing edge singularities, where $|\phi_x|$ is large.

Two fully implicit schemes are reported here that have no time step restriction based on a linear stability analysis. One scheme, an alternating-direction implicit algorithm, is applied to (4) in a manner similar to the Douglas-Gunn algorithm for the heat equation (ref. 5). The other scheme, an approximate factorization scheme, also factors difference approximations to (4) such that simple matrix solutions are required first in one spatial direction and then the other. In Section II, both schemes are investigated in terms of stability and accuracy for a model linear equation. In Section III, the shock capturing characteristics of the schemes are investigated, and conditions to prevent nonlinear instability and shock-capturing overshoots are found. In Section IV, the difference schemes are presented for the complete equation (4). Finally, in Section V the algorithms are applied and results compared for the simulated motion of a helicopter blade tip.

II. ALGORITHMS FOR THE MODEL LINEAR EQUATIONS

We begin by considering the model linear equation for (4)

$$\phi_{xt} = \beta\phi_{xx} + \phi_{yy} \tag{6}$$

An implicit differencing of (6) is sought to remove any time step restrictions other than those imposed by considerations of accuracy, and, for reasons of efficiency, computer-time consuming inversions must be avoided. The system of equations generated by implicit difference operators is perhaps most efficiently solved by structuring the difference operators so that they can be factored into easily inverted products. For simple difference equations one can sometimes construct fast direct solvers in this way, but as the complexity of the equations increases, approximate factorizations are usually sought. This is the concept of splitting and alternating directions (see, e.g., refs. 5, 6, and 7) which has recently been applied to the Eulerian gasdynamic equations (ref. 8). (The terminology "approximate factorization" is adopted from Yanenko (ref. 6, p. 27) and is perhaps the most descriptive name for this general class of procedures.) In this section two such procedures are developed which shall be referred to as a three-level approximate factorization (AF) scheme and a two-level alternating direction (ADI) scheme.

a) Approximate Factorization Algorithm

An implicit differencing of (6) for $\beta > 0$ is

$$\delta_{xt}\phi_{j,k}^{n+1} = \beta\delta_{xx}\phi_{j,k}^{n+1} + \delta_{yy}\phi_{j,k}^{n+1} \tag{7}$$

where

$$\delta_{xt} = (\Delta x \Delta t)^{-1}(1 - E_t^{-1})(1 - E_x^{-1}) \ , \qquad [0(\Delta t) + 0(\Delta x)] \tag{8a}$$

$$\delta_{xx} = (\Delta_{..})^{-2}(E_x^{-1} - 2 + E_x^{+1}) \ , \qquad [0(\Delta x^2)] \tag{8b}$$

$$\delta_{yy} = (\Delta y)^{-2}(E_y^{-1} - 2 + E_y^{+1}) \ , \qquad [0(\Delta y^2)] \tag{8c}$$

Here the shifting operators are defined by

$$\begin{aligned} E_t^{\pm 1}\phi_{j,k}^n &= \phi_{j,k}^{n\pm 1} \\ E_x^{\pm 1}\phi_{j,k}^n &= \phi_{j\pm 1,k}^n \\ E_y^{\pm 1}\phi_{j,k}^n &= \phi_{j,k\pm 1}^n \end{aligned} \tag{9}$$

with $t = n\Delta t$, $x = j\Delta x$, and $y = k\Delta y$. In the above, δ_{xt} is kept first-order accurate for simplicity — a second-order-accurate version will be described later. Note that (8b) can be rewritten $\delta_{xx} = (\Delta x)^{-2}(E_x^{+1} - 1)(1 - E_x^{-1})$.

Various factorizations of (7) are possible, but one that makes use of the common factor in δ_{xx} and δ_{xt} and requires only simple bidiagonal and tridiagonal inversions is

$$[1 - a(E_x^{+1} - 1)][1 - E_x^{-1} - b\delta_{yy}]\phi_{j,k}^{n+1} = [1 - E_x^{-1} + ab(E_x^{+1} - 1)\delta_{yy}]\phi_{j,k}^n \tag{10}$$

where $a = \beta \frac{\Delta t}{\Delta x}$ and $b = \Delta t \Delta x$. The approximate factorization (10) differs from (7) by the added cross term

$$[ab(E_x^{+1} - 1)\delta_{yy}][E_t^{+1} - 1]\phi_{j,k}^n = 0(\Delta x \Delta t^3 \phi_{xyyt}) \tag{11}$$

which, compared to the other terms, is of second order. Further, if a steady state is reached, the added cross term is zero.

The advantage of the AF form is that the inversion process is quite simple. As indicated in sketch (a) only bidiagonal and tridiagonal inversions are required, and the intermediate solution results can be overloaded into the same double array. A difficulty with the AF method is the need to supply the value $(1 - E_x^{-1} - b\delta_{yy})\phi_{J+1,k}^{n+1}$ as a boundary condition during the inversion of each upper bidiagonal. For example, if $\phi_{J+1,k}^{n+1}$ is given on the boundary, $\phi_{J,k}^{n+1}$ remains unknown, unless one can estimate ϕ_x on the downstream boundary. A simple approach is to use data at level n in place of the unknown $n+1$ boundary data. However, this particular approximation can impose conditional stability criteria, although not very stringent ones, especially if the local value of Δx is large.

Solution Procedure for equation (10) using a double array, $\phi^n_{j,k}$

Form right-hand side (overstore $\tilde{\phi}_{j,k}$ into $\phi^n_{j,k}$)

$$f_j = \delta_{yy}\phi^n_{j,k} \quad , \qquad , J+1$$

$$\tilde{\phi}_{j,k} = \phi^n_{j,k} - \phi^n_{j-1,k} + ab(f_{j+1} - f_j) \quad , \quad j = J,1$$

Inversion of first factor (overstore $\tilde{\tilde{\phi}}_{j,k}$ into $\phi^n_{j,k}$) $\qquad k = 1,K$

$$\tilde{\tilde{\phi}}_{j,k} = (\tilde{\phi}_{j,k} + a\tilde{\tilde{\phi}}_{j+1,k})/(1 + a) \quad , \quad j = J,1$$

with $\quad \tilde{\tilde{\phi}}_{J+1,k} \doteq (\phi^{n+1}_{J+1,k} - \phi^{n+1}_{J,k} - b\delta_{yy}\phi^{n+1}_{J+1,k})$

Tridiagonal inversion (overstore $\phi^{n+1}_{j,k}$ into $\phi^n_{j,k}$)

$$\phi^{n+1}_{j,k} - \frac{b}{(\Delta y)^2}(\phi^{n+1}_{j,k-1} - 2\phi^{n+1}_{j,k} + \phi^{n+1}_{j,k+1}) = \tilde{\tilde{\phi}}_{j,k} + \phi^{n+1}_{j-1,k} \quad , \quad k = 1,K \qquad j = 1,J$$

Sketch (a)

The algorithm (10) is unconditionally stable for $\beta > 0$ by a linear stability test (see Appendix A, part a, for details). If $\beta < 0$, the algorithm is modified so that δ_{xx} is the first-order three point backward difference operator, and stability is again unconditional. The AF algorithm for $\beta < 0$ is given by

$$[1 - a(1 - E_x^{-1})][1 - E_x^{-1} - b\delta_{yy}]\phi^{n+1}_{j,k} = [1 - E_x^{-1} + ab(1 - E_x^{-1})\delta_{yy}]\phi^n_{j,k} \qquad (12)$$

and the solution process is much as in sketch (a) — a lower-bidiagonal inversion replaces the upper-bidiagonal inversion, and boundary conditions are simplified.

Second-order accuracy in time can be obtained by using the following three level finite-difference operator for ϕ_{xt}

$$\delta_{xt} = (2\Delta t\Delta x)^{-1}[3 - E_t^{-1}(2 - E_x)](1 - E_t^{-1})(1 - E_x^{-1}) \quad , \qquad [0(\Delta t^2) + 0(\Delta x^2)] \qquad (13)$$

The operator (13) was derived by Taylor series expansion so that only the factor $(1 - E_x^{-1})$ appears at the n+1 level, and the factorization is much as before. The three-level scheme can be programmed so that only two levels of computer storage are required.

The extension of the AF algorithm to three dimensions is easily accomplished. For the equation

$$\phi_{xt} = \beta\phi_{xx} + \phi_{yy} + \phi_{zz} \tag{14}$$

an unconditionally stable approximate factorization using operators (8) with δ_{zz} similarly defined is given by

$$[1 - a(E_x^{+1} - 1)][(1 - b\delta_{yy})(1 - b\delta_{zz}) - E_x^{-1}]\phi_{j,k}^{n+1}$$

$$= [1 - E_x^{-1} + a(E_x^{+1} - 1)b(\delta_{yy} + \delta_{zz} - b\delta_{yy}\delta_{zz}) + b^2\delta_{yy}\delta_{zz}]\phi_{j,k}^{n} \tag{15}$$

The inversions are again straightforward, although a complicated cross term has to be computed at level n. In many problems the term $b^2\delta_{yy}\delta_{zz}$ could be safely neglected and always without losing second-order accuracy.

b) The Alternating-Direction Algorithm

A two time level differencing of (6) is given by

$$\delta_{xt}\phi_{j,k}^{n+1} = \frac{1}{2}(\beta\delta_{xx} + \delta_{yy})(\phi_{j,k}^{n+1} + \phi_{j,k}^{n}) \tag{16}$$

where the previous operators (8) are used; or, to maintain second-order accuracy

$$\delta_{xt} = (\Delta x\Delta t)^{-1}(1 - E_t^{-1})\left(\frac{3 - E_x^{-1}}{2}\right)(1 - E_x^{-1}) , \qquad [O(\Delta t^2) + O(\Delta x^2)] \tag{17}$$

An approximate factorization of (16) is obtained from the Douglas-Gunn alternating-direction algorithm with the identity operator replaced by δ_x as follows

$$\left(\delta_x - \frac{\Delta t}{2}\delta_{yy}\right)\tilde{\phi}_{j,k}^{n+1} = \left(\delta_x + \frac{\Delta t}{2}\delta_{yy} + \Delta t\beta\delta_{xx}\right)\phi_{j,k}^{n} \tag{18a}$$

$$\left(\delta_x - \frac{\Delta t}{2}\beta\delta_{xx}\right)\phi_{j,k}^{n+1} = \delta_x\tilde{\phi}_{j,k}^{n+1} - \frac{\Delta t}{2}\beta\delta_{xx}\phi_{j,k}^{n} \tag{18b}$$

where

$$\delta_x = (1 - E_x^{-1})/\Delta x \qquad \text{(first order)}$$

or

$$\delta_x = \left(\frac{3 - E_x^{-1}}{2}\right)\left(\frac{1 - E_x^{-1}}{\Delta x}\right) \qquad \text{(second order)}$$

The first step of this procedure is a consistent approximation to (6) and, in fact, is identical to the semi-implicit method of reference 4.

To show that (18) represents an approximate factorization to (16), insert $\delta_x^{-1}\delta_x = 1$ (the constant of summation is taken as zero) between $[\delta_x - (\Delta t/2)\delta_{yy}]$ and $\tilde{\phi}^{n+1}_{j,k}$ in (18a), and then eliminate $\delta_x\tilde{\phi}^{n+1}_{j,k}$ using (18b) with the result

$$(\delta_x - \frac{\Delta t}{2}\delta_{yy})\delta_x^{-1}[(\delta_x - \frac{\Delta t}{2}\beta\delta_{xx})\phi^{n+1}_{j,k} + \frac{\Delta t}{2}\beta\delta_{xx}\phi^{n}_{j,k}]$$

$$= (\delta_x + \frac{\Delta t}{2}\delta_{yy} + \Delta t\beta\delta_{xx})\phi^{n}_{j,k} \qquad (19)$$

Algebraically rearranging terms

$$(\delta_x - \frac{\Delta t}{2}\delta_{yy} - \frac{\Delta t}{2}\beta\delta_{xx})\phi^{n+1}_{j,k}$$

$$= (\delta_x + \frac{\Delta t}{2}\delta_{yy} + \frac{\Delta t}{2}\beta\delta_{xx})\phi^{n}_{j,k} - \left(\frac{\Delta t}{2}\right)^2\beta\delta_{yy}\delta_x^{-1}\delta_{xx}(1 - E_t^{-1})\phi^{n+1}_{j,k} \qquad (20)$$

With Δt divided out the error term is $O(\Delta t^2\phi_{yyxt})$ as for the AF scheme.

In the inversion procedure for (18), $\tilde{\phi}^{n+1}$ must be supplied as a boundary condition in step (18a). From step (18b) this means that

$$\tilde{\phi}^{n+1}_{j,k} = \phi^{n+1}_{j,k} - \frac{\Delta t}{2}\delta_x^{-1}\delta_{xx}(\phi^{n+1}_{j,k} - \phi^{n}_{j,k})$$

must be supplied on the boundaries, but to second-order accuracy $\tilde{\phi}^{n+1}_{j,k}$ can be taken as $\phi^{n+1}_{j,k}$ on the boundary. This is typical of the Douglas-Gunn method — implementation of other, even rearranged, approximate factorizations may require that the function and a derivative be specified on the boundary.

For $\beta > 0$, (18) is unconditionally stable by a linear stability test (see Appendix A, part b). For $\beta < 0$, δ_{xx} is backward differenced to maintain stability, and the first-order three-point backward difference is used. The scheme generalizes to three dimensions in the usual Douglas-Gunn-like fashion with the δ_x operator replacing the usual identity operator. Finally, it is remarked that this procedure generalizes to any number of operators in time that contain the factor $(1 - E_t^{-1})$. For example, if, as in differencing (1), an operator such as $(1 - E_t^{-1})\mathcal{L}(\delta_x,\delta_t)\phi^{n+1}_{j,k}$ appears, the operator $\mathcal{L}(\delta_x,\delta_t)$ replaces the usual identity operator of the Douglas-Gunn algorithm. Of course, stability is not generally ensured.

c) A Numerical Verification of the Linear Algorithms

The following example is presented as a simple check on the accuracy and stability of the implicit schemes. The motion is that of a parabolic arc airfoil increasing its thickness from zero to 0.1, according to the relation shown in figure 2, in the time it takes a fluid particle to travel fifteen chord lengths at the free-stream velocity U_∞. Since the motion is not periodic, t is scaled by c/U_∞ rather than $1/\omega$. This is equivalent to

taking $k = 1$ in (4) so that time is given in chord lengths traveled rather than radians. Solutions of the linear version of (4) (i.e., $\gamma = -1$) are compared in figure 2 in terms of pressure coefficient, $C_p = -2\phi_x$, at $x = 0.525$ as computed from the second-order ADI scheme and from linear theory (exact). Equivalent results were obtained with the second order AF scheme. Here the x grid spacing was uniform at $\Delta x = 0.05$ chord lengths. The vertical mesh spacing, also uniform, was 0.1. The time step was five times greater than that permitted by the semi-implicit scheme (see (5)), and no accuracy or stability problems were encountered.

III. ONE-DIMENSIONAL SHOCK WAVE MOTION

a) Model Problem

The shock capturing properties of the implicit finite-difference schemes can be investigated using the inviscid Burger's equation, given here in terms of the velocity potential

$$(\phi_x)_t + (\phi_x^2)_x = 0 \tag{21}$$

along with boundary and initial conditions

$$\phi(0,t) = 0 , \quad \phi_x(0,t) = \phi_{x_L} , \quad \phi_x(\ell,t) = \phi_{x_R}$$

$$\phi(x,0) = \begin{cases} \phi_{x_L} \cdot x , & 0 \le x \le x_{s_o} \\ \phi_{x_L} \cdot x_{s_o} + \phi_{x_R}(x - x_{s_o}) , & x_{s_o} \le x \le \ell \end{cases} \tag{22}$$

The initial conditions are sketched in figure 3. The solution to (21) and (22) is $\phi_x = \phi_{x_L}$ for $x < x_s$ and $\phi_x = \phi_{x_R}$ for $x > x_s$, where x_s is the instantaneous location of the shock wave and is given by $x_s = x_{s_o} + (\phi_{x_L} + \phi_{x_R})t$ (here we exclude so-called "expansion shocks"). The potential ϕ must be continuous for all x,t.

b) Difference Schemes

Equation (21) is written in difference form as

$$\delta_{xt}\phi^{n+1}_{j,k} + D_x f_j = 0 \tag{23}$$

where

$$f_j = f(\phi^{n+1}_{x_j}, \phi^{n}_{x_j})$$

and

$$\phi_{x_j} = [\phi_{j+(1/2)} - \phi_{j-(1/2)}]/\Delta x$$

The quantity f_j is some difference approximation for $(\phi_x)^2$, and the difference operator D_x remains to be specified. To avoid iteration at the n+1 level, f_j is linearized by expanding in terms of $\phi^{n+1}_{x_j}$. For the AF scheme, $\phi_x{}^2$ is evaluated at time level n+1, and the following first- and second-order linearizations can be made

$$f_{AF_j} = (\phi^{n+1}_{x_j})^2 = \phi^n_{x_j}\phi^{n+1}_{x_j} + 0(\Delta t) \tag{24a}$$

(and by Taylor series expansion)

$$f_{AF_j} = (\phi^{n+1}_{x_j})^2 = (\phi^n_{x_j})^2 + 2\phi^n_{x_j}(\phi^{n+1}_{x_j} - \phi^n_{x_j}) + 0(\Delta t^2) \tag{24b}$$

For the ADI scheme, ϕ_x is averaged at the n and n+1 time levels, which, along with (24b), gives

$$f_{ADI_j} = \frac{1}{2}[(\phi^{n+1}_{x_j})^2 + (\phi^n_{x_j})^2] = \phi^n_{x_j}\phi^{n+1}_{x_j} + 0(\Delta t^2) \tag{24c}$$

(The use of the terms "AF" and "ADI" is strictly not correct in this one-dimensional application, but the terminology is convenient in relationship to the subsequent development of the two-dimensional algorithms.)

In Section II it was determined that central and backward differences for ϕ_{xx} were required to maintain stability for the cases $\beta > 0$ (subsonic) and $\beta < 0$ (supersonic), respectively. In differencing (23) then, central and backward differences should be used for f when $\phi_x < 0$ (subsonic) and $\phi_x > 0$ (supersonic), respectively. As shown by Murman (ref. 9), care must be taken in switching from one difference operator to another, otherwise the conservative form and its correct weak solution may not be maintained. Switched differences can be used while maintaining proper conservation form by expressing D_x in the form

$$D_x f_j = \left\{(1 - \epsilon_j)[f_{j+(1/2)} - f_{j-(1/2)}] + \epsilon_{j-1}[f_{j-(1/2)} - f_{j-(3/2)}]\right\}\Big/\Delta x \tag{25}$$

with $\epsilon_j = 0$ or 1 for $(\phi^n_{j+1} - \phi^n_{j-1})$ less or greater than zero. In Murman's terminology

$$\begin{aligned}
&\epsilon_{j-1} = 0\ ,\ \epsilon_j = 0 \Rightarrow \text{subsonic point}\\
&\epsilon_{j-1} = 1\ ,\ \epsilon_j = 1 \Rightarrow \text{supersonic point}\\
&\epsilon_{j-1} = 1\ ,\ \epsilon_j = 0 \Rightarrow \text{shock point}\\
&\epsilon_{j-1} = 0\ ,\ \epsilon_j = 1 \Rightarrow \text{parabolic (or sonic) point}
\end{aligned} \tag{26}$$

The procedure used here to maintain conservation form with switched differences can be summarized as follows: write the difference equation in conservation form as in (23), linearize as in (24), then apply the switching operator D_x as in (25). Violation of this procedure can result in nonconservative difference schemes which yield erroneous shock speeds, as demonstrated in Appendix B.

Using time linearizations consistent with the order of δ_{xt}, first- and second-order accurate implicit differences for (21) are given by

First order AF and ADI

$$\phi_j^{n+1} - \phi_{j-1}^{n+1} = -\Delta x \Delta t D_x(\phi_{x_j}^n \phi_{x_j}^{n+1}) + \phi_j^n - \phi_{j-1}^n \tag{27a}$$

Second order ADI (two level)

$$3\phi_j^{n+1} - 4\phi_{j-1}^{n+1} + \phi_{j-2}^{n+1} = -2\Delta x \Delta t D_x(\phi_{x_j}^n \phi_{x_j}^{n+1}) + 3\phi_j^n - 4\phi_{j-1}^n + \phi_{j-2}^n \tag{27b}$$

Second order AF (three level)

$$\begin{aligned} 3(\phi_j^{n+1} - \phi_{j-1}^{n+1}) = {} & -2\Delta x \Delta t D_x[\phi_{x_j}^n (2\phi_{x_j}^{n+1} - \phi_{x_j}^n)] \\ & - (5\phi_{j-1}^n - 6\phi_j^n + \phi_{j+1}^n) + 2\phi_{j-1}^{n-1} - 3\phi_j^{n-1} + \phi_{j+1}^{n-1} \end{aligned} \tag{27c}$$

Note that the first-order AF and ADI schemes are equivalent. Also, the term "second order" in (27b) and (27c) applies only for locally subsonic regions because the upwind difference used in $D_x f_j$ for locally supersonic flows is only first-order accurate.

For purposes of comparison, the semi-implicit scheme of reference 4 is

$$\phi_j^{n+1} - \phi_{j-1}^{n+1} = -\Delta x \Delta t D_x(\phi_{x_j}^n)^2 + \phi_j^n - \phi_{j-1}^n \tag{28}$$

and it is subject to the stability criterion $\Delta t \leq \Delta x/(2|\phi_x|_{max})$.

c) Shock Characterization

To investigate the shock-capturing characteristics of the numerical schemes, four types of shock motions are considered, as summarized in table I. The terms "subsonic" and "supersonic" are relative to the coordinate system and not to the moving shock.

TABLE I.- CLASSIFICATION OF SHOCK MOTIONS

Shock	Characteristic	Spatial differencing
1. Supersonic-to-supersonic	$\phi_{x_L} > 0,\ \phi_{x_R} > 0$	Backward
2. Subsonic-to-subsonic	$\phi_{x_L} < 0,\ \phi_{x_R} < 0$	Central
3. Supersonic-to-subsonic (downstream moving)	$\phi_{x_L} + \phi_{x_R} > 0, \phi_{x_R} < 0$	Mixed
4. Supersonic-to-subsonic (upstream moving)	$\phi_{x_L} + \phi_{x_R} < 0, \phi_{x_R} < 0$	Mixed

A parameter that has a significant effect on the shock capturing properties of any one of the schemes is the number of Δx increments the shock wave travels in a time Δt

$$T \equiv \frac{\Delta t}{\Delta x} \frac{dx_s}{dt} \tag{29}$$

where the correct shock speed for (21) is $dx_s/dt = (\phi_{x_L} + \phi_{x_R})$, and a uniform grid is assumed. A value $T > 1$ corresponds to the case where the shock moves a distance of one grid point per time step. Another parameter of interest is the Courant number

$$\nu = 2|\phi_x|\frac{\Delta t}{\Delta x} \tag{30}$$

and the stability restriction for the semi-implicit scheme is $|\nu| \leq 1$.

d) Computed Results

Now consider the implicit schemes (27) applied to the model problem (21) with initial conditions (22) for the first type of shock motion listed in table I, the supersonic-to-supersonic case. In this case the term $(\phi_x{}^2)_x$ is approximated by backward differences throughout. Results of the first-order (27a), second-order ADI (27b), and second-order AF (27c) schemes are compared in figure 4. Results from each of the schemes are shown at two values of T for the same time. The shock profiles shown remain essentially unchanged for all greater times. The exact solution is given by the dashed lines, and the shock location is indicated by x_s.

Results for the second type of shock motion, the subsonic-to-subsonic case, are shown in figure 5. In this case the term $(\phi_x{}^2)_x$ is approximated by central differences throughout. Again the shock profiles shown remain essentially the same for all larger n. The first-order results are similar

in appearance to those for the supersonic-to-supersonic case. The second-order results contain oscillations that increase with T.

A sequence of shock profiles for an upstream-moving, supersonic-to-subsonic shock is shown in figure 6. For the supersonic-to-subsonic cases, mixed differences are used for $(\phi_x{}^2)_x$. The sequence of shock profiles is periodic, repeating every fifth time step, because $T = 0.2$. All the schemes capture the shock sharply, but again oscillations are apparent in the second-order schemes. Similar results are shown in figure 7 for a downstream moving, supersonic-to-subsonic shock.

The first-order results of figure 7 are replotted in terms of ϕ vs. x in figure 8. The dashed lines indicate the exact solution at different time steps. The exact shock location at time level n is indicated by the intersection of two dashed lines and is marked by x_{s_n} on the abscissa. The location of the shock relative to the mesh at $n = 19$ is repeated at $n = 24$, and that at $n = 20$ is repeated at $n = 25$, etc. Points identified as shock points at level n according to (26) are denoted by S_n. The solution to the difference equation (27a) for the case treated in figure 8 is

$$\left.\begin{aligned} \phi_j^{n+1} &= \phi_j^n \quad \text{for} \quad x_j < x_{s_n} \\ \phi_j^{n+1} &= \phi_j^n - \Delta x_s\left(\phi_{x_R} - \phi_{x_L}\right) \quad \text{for} \quad x_j \geq x_{s_n} \end{aligned}\right\} \tag{31}$$

where Δx_s, the distance the shock travels in time Δt, is given by $\Delta x_s = \Delta t(\phi_{x_L} + \phi_{x_R})$. Hence, in updating ϕ from time level n to $n+1$, the solution remains unchanged for all (supersonic) points to the left of the shock point. The shock point, and all (subsonic) points to the right of it, move to the dashed line that is the exact solution for $n + 1$. The test to determine S_n assures that the shock point remains downstream of the shock for the value of T used here.

e) Nonlinear Instability and Overshoots

For large values of T, however, the shock-capturing procedure breaks down, and an instability occurs as illustrated in figure 9. Here the solution downstream of the exact shock location is correct for each n, because of the test for S_n, the shock point can move only one grid point downstream per time step, while for $T = 2$, the exact shock location moves downstream at a rate of two grid points per time step. An increasingly large discontinuity in ϕ develops, which appears as a growing overshoot in ϕ_x, and the process diverges. Reducing T to 1.1 slows the divergence rate, as illustrated in figure 10. For $T = 1.0$, the process is neutrally stable, as shown in figure 11, and the ϕ_x vs. x shock profile travels unattenuated after $n = 3$. For the case $T = 0.9$, shown in figure 12, no instability occurs. The sequence is periodic with the solution repeating every tenth time step. An overshoot develops at $n = 1$ that decays with n until it repeats at $n = 11$.

For this type of switched-differencing-induced overshoot to occur, two conditions must be met: (1) the point immediately downstream of the shock must be a shock point, and (2) the (downstream moving) shock must move past this point in the next time step. Referring to figure 3, these conditions can be expressed, respectively, as

$$\phi_{j_{s+1}} - \phi_{j_{s-1}} < 0 \Rightarrow x_{j_s} - x_{s_o} > \Delta x \left(\frac{\phi_{x_L} + \phi_{x_R}}{\phi_{x_L} - \phi_{x_R}} \right) \tag{32a}$$

$$x_{j_s} - x_{s_o} < \Delta t(\phi_{x_L} + \phi_{x_R}) \tag{32b}$$

or, equivalently,

$$\frac{T(\Delta x/\Delta t)}{\phi_{x_L} - \phi_{x_R}} < \frac{x_{j_s} - x_{s_o}}{\Delta x} < T \tag{32c}$$

This indicates that the occurrence of overshoots depends on the speed of the shock and its location relative to the mesh. As the shock propagates through the grid, (32c) may be satisfied at some time levels and not at others. It follows from (32c) that these overshoots can never occur if

$$T \equiv \frac{\Delta t}{\Delta x}\left(\phi_{x_L} + \phi_{x_R}\right) < \frac{\phi_{x_L} + \phi_{x_R}}{\phi_{x_L} - \phi_{x_R}} \tag{33}$$

This is a more restrictive condition than the $T \leq 1$ requirement for stability. Inequalities can be derived from the upstream-moving shock case in a similar way.

The type of instability and overshoot discussed here cannot occur in the semi-implicit scheme, because, for a downstream-moving supersonic-to-subsonic shock, the linear stability condition is more restrictive than the inequality (33). It is also interesting to note that for the nonconservative (in time) scheme detailed in the appendix, no overshoots or instabilities occur.

For the implicit schemes presented here, the shock-capturing process imposes time step limitations for both stability (due to the time linearization of the nonlinear term) and accuracy. The restriction $T \leq 1$ could be eliminated by fitting the shock as an internal boundary. Alternately, the following simple correction process could perhaps be implemented. First, update ϕ at $n+1$ by applying the implicit scheme as before. However, before proceeding to the next time step, any points crossed by the shock in time Δt would be corrected, i.e., they would be forced to lie on extrapolated curves from the upstream or downstream direction depending on the direction of shock travel. This procedure has been successfully applied in the one-dimensional case but has not yet been attempted in two-dimensions.

IV. NUMERICAL ALGORITHMS FOR THE LOW-FREQUENCY TRANSONIC EQUATION

The factored schemes introduced in Section II are combined here with the nonlinear mixed difference operators of Section III to form a complete algorithm for solving (4).

a) Alternating Direction Algorithm

An implicit differencing of the low-frequency, transonic, small-perturbation equation (4), using two time levels, can be denoted

$$\beta_1 \delta_{xt} \phi^{n+1}_{j,k} = \frac{1}{2}\,(1 + E_t^{-1})\left(D_x f^{n+1}_{j,k} + \delta_{yy}\phi^{n+1}_{j,k}\right) \tag{34}$$

where $\beta_1 \equiv 2kM_\infty{}^2$, D_x is defined by (40), and the difference operators for δ_{yy} and δ_{xt} are specified by the relations

$$\delta_{yy} = \left(\frac{E_y^{+1} - 1}{y_{k+1} - y_k} - \frac{1 - E_y^{-1}}{y_k - y_{k-1}}\right)\left(\frac{2}{y_{k+1} - y_{k-1}}\right) \tag{35a}$$

$$\delta_{xt} = \left(\frac{1 - E_t^{-1}}{\Delta t}\right)\left(\frac{1 - E_x^{-1}}{x_{j+1} - x_{j-1}}\right)\left[2 + \mu(1 - E_x^{-1})\right] = (\Delta t)^{-1}(1 - E_t^{-1})\delta_x \tag{35b}$$

Here $\mu = 0,1$ for the first- and second-order differences, respectively. The unusual choice of $(x_{j+1} - x_{j-1})$ used with the δ_{xt} operator is required to maintain conservation form for variable meshes. The operator (35b) is not the usual spatial second-order-accurate relation derived from a Taylor series expansion, but, for a sufficiently smooth grid variation, the difference is nevertheless second-order accurate. For example, introduce $\xi = \xi(x)$ with one to one mapping $x = x(\xi)$ such that $\xi_j - \xi_{j-1} = \Delta\xi$ is constant over the grid, and for the three-point backward spatial operator

$$\frac{(1 - E_x^{-1})(3 - E_x^{-1})}{x_{j+1} - x_{j-1}}\,\phi_j \approx \frac{(1 - E_x^{-1})(3 - E_x^{-1})\phi_j}{2\Delta\xi x_\xi + \frac{1}{3}\,(\Delta\xi)^2 x_{\xi\xi\xi} + \ldots} \approx \left[\phi_\xi + O(\Delta\xi^2)\right]\left[\xi_x - O(\Delta\xi^2)\right] \tag{36}$$

where $x_{j\pm1}(\xi)$ is expanded about $x_j(\xi)$ via Taylor series.

In (34)

$$f^{n+1}_{j,k} = \left[1 - M_\infty^2 - \frac{1}{2}\,(\gamma + 1)M_\infty^m \phi^{n+1}_{x_{j,k}}\right]\phi^{n+1}_{x_{j,k}} \tag{37}$$

where

$$\phi^n_{x_{j,k}} = \left[\phi^n_{j+(1/2),k} - \phi^n_{j-(1/2),k}\right]/\left[x_{j+(1/2)} - x_{j-(1/2)}\right]$$

Linearizing as in Section III gives

$$f^{n+1}_{j,k} = f^{n}_{j,k} + \left(\frac{\partial f}{\partial \phi_x}\right)^{n}_{j,k}\left(\phi^{n+1}_{x_{j,k}} - \phi^{n}_{x_{j,k}}\right) + \cdots \tag{38}$$

Two-time level averaging then gives

$$\begin{aligned}\bar{f}_{j,k} &= \bar{f}\left(\phi^{n}_{x_{j,k}}, \phi^{n+1}_{x_{j,k}}\right) = \frac{1}{2}\left(f^{n+1}_{j,k} + f^{n}_{j,k}\right) \\ &= \frac{1}{2}\left[V^{n}_{j,k}\phi^{n+1}_{x_{j,k}} + (1 - M_\infty^2)\phi^{n}_{x_{j,k}}\right]\end{aligned} \tag{39}$$

where

$$V^{n}_{j,k} = 1 - M_\infty^2 - (\gamma + 1)M_\infty^m \phi^{n}_{x_{j,k}}$$

The D_x operator is applied as in Section III

$$\begin{aligned}D_x\bar{f}_{j,k} = 2(x_{j+1} - x_{j-1})^{-1}\Big\{&(1 - \varepsilon_j)\left[\bar{f}_{j+(1/2),k} - \bar{f}_{j-(1/2),k}\right] \\ &+ \varepsilon_{j-1}\left[\bar{f}_{j-(1/2),k} - \bar{f}_{j-(3/2),k}\right]\Big\}\end{aligned} \tag{40}$$

where $\varepsilon_j = 0$ or 1 for $(V^{n}_{j+(1/2),k} + V^{n}_{j-(1/2),k}) > 0$ or < 0. (The same smooth grid restriction (36) applies to the case $\varepsilon_j = 1$.)

Incorporating the above differences in the ADI algorithm gives

x sweep

$$\beta_1(\Delta t)^{-1}\delta_x\left(\tilde{\phi}^{n+1}_{j,k} - \phi^{n}_{j,k}\right) = D_x\bar{f}_{j,k} + \delta_{yy}\phi^{n}_{j,k}$$

y sweep

$$\beta_1(\Delta t)^{-1}\delta_x\left(\phi^{n+1}_{j,k} - \tilde{\phi}^{n+1}_{j,k}\right) = \frac{1}{2}\,\delta_{yy}\left(\phi^{n+1}_{j,k} - \phi^{n}_{j,k}\right) \tag{41}$$

where $\bar{f}_{j,k} = \bar{f}(\phi^{n}_{x_{j,k}}, \tilde{\phi}^{n+1}_{x_{j,k}})$. On the x sweep, a matrix is generated that is lower tridiagonal for supersonic points ($\varepsilon_{j-1} = \varepsilon_j = 1$) and tridiagonal for subsonic points ($\varepsilon_{j-1} = \varepsilon_j = 0$). For parabolic points ($\varepsilon_{j-1} = 0$, $\varepsilon_j = 1$) all the entries are zero on the row, and for shock points ($\varepsilon_{j-1} = 1$, $\varepsilon_j = 0$), there are four nonzero entries on the row. For the present work, a quadradiagonal solver was used that solves the equations like the Thomas algorithm for a tridiagonal matrix. On the y sweep, the only x differences are in δ_{xx}, which is backward differenced. Hence, the scheme is marched from upstream to downstream solving a tridiagonal matrix for each x = constant line of y

grid points. The test for ϵ_j is only required for the x sweep. Had the y sweep been taken first here, as in Section II, the test would have been required on both sweeps, thereby reducing the computer efficiency of the method.

b) Approximate Factorization Algorithm

For the AF scheme the conservativ time-space differencing was carried out in the transformed potential

$$\tilde{\phi} = -\beta_2 x + (\gamma + 1)M_\infty^m \phi \tag{42}$$

so that the resulting equation

$$\beta_1 \tilde{\phi}_{xt} = -(\tilde{\phi}_x^2/2)_x + \tilde{\phi}_{yy} \tag{43}$$

has the same nonlinear term modeled in Section III. The use of such a transform is unnecessary for the basic scheme described below but does lead to some computational simplifications. The transform also avoids a difficulty with certain contrived time-linearizations such as $(\phi_{x_{j,k}}^{n+1})^2 \approx (2\phi_{x_{j,k}}^{n} - \phi_{x_{j,k}}^{n-1})\phi_{x_{j,k}}^{n+1}$ in which the switching of difference operators for numerical stability does not correspond to the correct sonic line. For example, use of this linearization in (37) leads to a coefficient of $\phi_{x_{j,k}}^{n+1}$ that changes sign at a different point than $V_{j,k}^n$.

Variable grid differencing was implemented in the AF scheme by coordinate stretching transforms, although the algorithm is given here in the untransformed plane. Using the second-order time linearization (24b) and mixed differencing (25) described in Section III, the second-order AF algorithm is given by

$$\begin{aligned}
&[1 + \Delta\hat{t}F_{j,k}^n/(3M_\infty^2)][6M_\infty^2\hat{\eta}_k^{-1}(1 - E_x^{-1}) - 2\Delta\hat{t}\hat{\xi}_j^{-1}\hat{\delta}_{yy}]\tilde{\phi}_{j,k}^{n+1} \\
&\quad = 2M_\infty^2\hat{\eta}_k^{-1}\left[(-5E_x^{-1} + 6 - E_x^{+1})\tilde{\phi}_{j,k}^{n} + (2E_x^{-1} - 3 + E_x^{+1})\tilde{\phi}_{j,k}^{n-1}\right] \\
&\quad\quad + 2\Delta\hat{t}F_{j,k}^n\left\{[\Delta\hat{t}\hat{\xi}_j^{-1}/(3M_\infty^2)]\hat{\delta}_{yy} + \tfrac{1}{2}\hat{\eta}_k^{-1}(1 - E_x^{-1})\right\}\tilde{\phi}_{j,k}^{n}
\end{aligned} \tag{44}$$

where

$$\hat{t} = t/k$$

$$\eta_k = (y_k - y_{k-1})^{-1}, \qquad \hat{\eta}_k = (\eta_{k+1} + \eta_k)/2$$

$$\xi_j = (x_j - x_{j-1})^{-1}, \qquad \hat{\xi}_j = (\xi_{j+1} + \xi_j)/2$$

$$F^n_{j,k} \equiv (1 - \varepsilon_j)\xi^2_{j+1}(\tilde{\phi}^n_{j+1,k} - \tilde{\phi}^n_{j,k})E_x^{+1} - (1 - \varepsilon_j - \varepsilon_{j-1})\xi^2_j(\tilde{\phi}^n_{j,k} - \tilde{\phi}^n_{j-1,k})$$

$$- \varepsilon_{j-1}\xi^2_{j-1}(\tilde{\phi}^n_{j-1,k} - \tilde{\phi}^n_{j-2,k})E_x^{-1}$$

and

$$\hat{\delta}_{yy} = \eta_{k+1}(E_y^{+1} - 1) - \eta_k(1 - E_y^{-1})$$

The above algorithm only requires two double-indexed storage arrays with intermediate values held in $\tilde{\phi}^{n-1}_{j,k}$. For efficiency, the operator $F^n_{j,k}$ should be simultaneously computed along rows for the right-hand side and the first inversion. In forming $F^n_{j,k}$ along rows, the term $\xi^2_{j+1}(\tilde{\phi}^n_{j+1,k} - \tilde{\phi}^n_{j,k})$ is computed and then shifted back to obtain $\xi^2_j(\tilde{\phi}^n_{j,k} - \tilde{\phi}^n_{j-1,k})$ and $\xi^2_{j-1}(\tilde{\phi}^n_{j-1,k} - \tilde{\phi}^n_{j-2,k})$. If only a first-order-accurate differencing for $\tilde{\phi}_{x\tau}$ is needed (i.e., (8a)), the simplified contrived time linearization (24a) should be used.

V. SAMPLE TWO-DIMENSIONAL COMPUTATION

In this section results from the ADI and AF schemes are compared for the case of an airfoil executing unsteady motion characteristic of a helicopter rotor in forward flight. Particular attention is directed toward comparing the shock capturing properties of the first- and second-order methods for various types of shock motion in light of the one-dimensional results presented in Section III. For the computations reported in this section, a uniform x mesh spacing of $\Delta x = 0.02$ chord lengths was maintained over a distance extending from one chord length upstream of the airfoil to the airfoil trailing edge. The x mesh spacing outside this interval was stretched smoothly out to the boundaries, which were located more than thirty chord lengths from the airfoil. The mesh spacing in the stream-normal direction was uniform at $\Delta y = 0.04$ (y unscaled), starting at the airfoil surface and extending for a distance of 0.2 chord lengths. It was stretched smoothly beyond this point out to the grid boundary, which was located a distance of fifty chord lengths from the airfoil.

The motion of a blade element near the tip of an advancing helicopter rotor can be simulated by an accelerating, and, subsequently decelerating, airfoil (refs. 2 and 10). A motion that is simpler to treat computationally, but which produces a similar flowfield, is that of a thickening-thinning airfoil as shown in figure 13. A parabolic-arc airfoil thickens from zero to 0.1 in the time interval in which a fluid particle travels fifteen chord lengths (relative to the airfoil) at the free-stream velocity U_∞. The airfoil then thins to a flat plate after thirty chord lengths of travel. (Here $k = 1$ as in Section IIc, so time is given in chord lengths of free-stream travel.) During the thickening phase of the motion, a shock wave forms and propagates downstream. As the airfoil thins, the shock reverses, moves upstream, and propagates off the front of the airfoil chasing the expansion wave that

precedes it. The initial formation and downstream propagation of the shock wave is indicated by the pressure distributions shown in figure 14. The second-order ADI and AF schemes show no plottable difference.

An indication of the shock speed can be obtained from the jump relations for (4). For a normal shock, the speed is given by $(1/2kM_\infty^2)[1 - M_\infty^2 + (1/2)(\gamma + 1)M_\infty^m(C_{p_L} + C_{p_R})/2]$ (where $C_p = -2\phi_x$), and, in transonic small-disturbance theory, C_p^* is given by setting $V_c = 0$ in (1) or (4), i.e., $1 - M_\infty^2 + (1/2)(\gamma + 1)M_\infty^m C_p^* = 0$. Hence, when the average C_p across the shock is equal to C_p^*, the shock is stationary; otherwise the difference between $(C_{p_L} + C_{p_R})/2$ and C_p^* indicates the direction and speed of the shock. Thus, at $t = 11.5$, the shock is traveling downstream, while at $t = 18.25$, it is nearly stationary. As in Section III, this downstream-moving supersonic-to-subsonic shock is properly captured, and the ADI and AF schemes give equivalent results.

The subsequent upstream movement of the shock wave is shown in figure 15. At $t = 26.875$, there is only a small region of supersonic flow (for which $C_p < C_p^*$), and the shock is traveling rapidly upstream. Here, as in Section III, the upstream-moving supersonic-to-subsonic shock wave produces overshoots in the second-order scheme results. At later times, the shock is a subsonic-to-subsonic type, and it is accelerating in the upstream direction, as indicated by the increasingly large ratio of $|(C_{p_L} + C_{p_R})/2C_p^*|$ as a function of time. Here, as in Section III, the first-order schemes produce some "smearing" while the second-order schemes develop overshoots. Halving the time step reduced the amplitude of these oscillations in the second-order solutions and produced no plottable difference in the first-order solutions.

Another view of the solution is afforded by the mid-chord pressure coefficients as a function of time as shown in figure 16. There is a lag of about two chord lengths between the maximum flow expansion point and the maximum airfoil thickness. The effect of the shock wave propagating upstream past the mid-chord point is evident at about $t = 26$.

It is interesting to compare the relative efficiencies of the implicit and semi-implicit schemes for the present example and to try to extrapolate the results of such a comparison to cases of more practical interest. In the present calculations, Δt was fixed at $\Delta t = 0.125$, where time is given here in chord lengths of free-stream travel relative to the airfoil. Considerably larger time steps could have been taken over much of the period of the motion, the major restriction being adequate resolution of the rapid shock motion upstream of the airfoil. The time step restriction for the semi-implicit scheme is given by

$$\Delta t \leq \mathrm{Min}_{j,k}\left[\frac{2M_\infty^2 \Delta x}{\left|1 - M_\infty^2 + \frac{\gamma + 1}{2} M_\infty^m C_{p_{j,k}}\right|}\right] \tag{45}$$

where the minimum is taken over all spatial grid points j,k in the flowfield. In the present calculations, the most restrictive Δt according to

(45) would be $\Delta t = 0.0328$ at $t \approx 16$. Since the implicit schemes require about fifty percent more work per time step, the efficiency ratio of the implicit schemes relative to the semi-implicit schemes is roughly 2.5 for this case. In more practical cases, i.e., for blunt leading-edge airfoils at angle of attack (e.g., see ref. 3), the leading edge singularity is much stronger, and a much finer Δx is required in the nose region. (The solution is not a valid approximation to the Euler equations in this region because of the violation of the small-disturbance assumptions under which the theory is derived. However, experience indicates that for sufficiently fine grids near the leading edge, these inaccuracies are confined to a small region, whereas for coarser grids, they can affect the solution over the entire surface of the airfoil.) Small Δx and large C_p both contribute to a considerably more severe time-step restriction for such cases, significantly increasing the efficiency ratio in favor of the implicit schemes.

CONCLUDING REMARKS

Implicit two- and three-level approximate factorization finite-difference schemes for the low-frequency transonic small-disturbance equation have been constructed that have no time-step limitation based on a linear stability analysis. At this point neither scheme appears to be superior to the other either in terms of accuracy or efficiency, and the development and application of both will continue. Both schemes maintain stability for mixed flows by the use of conservatively-switched differences, i.e., central or backward differences are used as the local flow condition is subsonic or supersonic. An instability, caused by the time linearization and switching test, occurs whenever a shock wave travels more than one spatial grid point per time step. A mild time-step restriction is thus imposed that is usually orders of magnitude less severe than the one associated with explicit schemes. The implicit schemes should prove useful in the analysis of unsteady airfoil motions, including pitch, plunge and free-stream Mach number oscillations; and the extension to three dimensions, as outlined in Section II, should present no additional difficulty.

ACKNOWLEDGMENT

The authors wish to thank Mr. John Albert, a student at Santa Clara University, for his programming efforts contributing to the results presented in Section III.

APPENDIX A

a) Stability of the AF Scheme

To investigate the stability of (10) simplified boundary conditions are taken as either (a) spatial periodicity, or, because the all periodic case leads to a singular factor $[(1 - E_x^{-1}) - b\delta_{yy}]$, (b) spatial periodicity in x and specified function on the y boundaries. If $\vec{\phi}$ is the JxK vector ordered $\phi_{j,k}$ $[(j = 1, J), k = 1, k]$ then (10) can be written

$$AB\vec{\phi}^{n+1} = C\vec{\phi}^{n} + \vec{f}$$

The matrices A, B and C are either block diagonal or block tridiagonal with circulant blocks (because of periodicity in x) and can be simultaneously diagonalized by unitary transforms. Hence, in an ℓ_2-norm one need only examine the eigenvalues for stability. For the periodic boundary condition case, the difference operators generate circulant matrices with known eigenvalues (refs. 11 and 12), and the matrix stability test is equivalent to the von Neumann test. Thus (10) is transformed

$$(1 + a - ae^{i\theta_j})\left[1 - e^{-i\theta_j} + 4C \sin^2\left(\frac{\theta_k}{2}\right)\right]\tilde{\phi}^{n+1}_{j,k} = \left\{1 - e^{-i\theta_j} + ac(e^{i\theta_j} - 1)\left[-4 \sin^2\left(\frac{\theta_k}{2}\right)\right]\right\}\tilde{\phi}^{n}_{j,k} \qquad (A1)$$

where $c = b/(\Delta y)^2$ and $\theta_j = 2\pi j/J$, $\theta_k = 2\pi k/K$, or $\theta_k = 2\pi k/(K + 1)$ if the function is specified at end points in y. This can be regrouped as

$$\left\{\left(1 - e^{-i\theta_j}\right) + ac\left(1 - e^{i\theta_j}\right)\left[4 \sin^2\left(\frac{\theta_k}{2}\right)\right] + a\left(1 - e^{i\theta_j}\right)\left(1 - e^{-i\theta_j}\right) + 4c \sin^2\left(\frac{\theta_k}{2}\right)\right\}\tilde{\phi}^{n+1}_{j,k} = \left\{1 - e^{-i\theta_j} + ac\left(1 - e^{i\theta_j}\right)\left[4 \sin^2\left(\frac{\theta_k}{2}\right)\right]\right\}\tilde{\phi}^{n}_{j,k} \qquad (A2)$$

Now

$$a\left(1 - e^{-i\theta_j}\right)\left(1 - e^{i\theta_j}\right) = 4a \sin^2\left(\frac{\theta_j}{2}\right) \geq 0 \text{ and } 4c \sin^2\left(\frac{\theta_k}{2}\right) \geq 0$$

so (A2) has the form

$$\tilde{\phi}^{n+1}_{j,k} = \frac{\hat{a} + ic}{a + ic}\,\tilde{\phi}^{n}_{j,k} = \sqrt{\frac{\hat{a}^2 + c^2}{a^2 + c^2}}\, e^{i\omega}\tilde{\phi}^{n}_{j,k} \qquad (A3)$$

Since $a \geq \hat{a} > 0$, $|\tilde{\phi}^{n+1}_{j,k}| > |\tilde{\phi}^{n}_{j,k}|$, and unconditional stability is assured, although in the periodic case when $j = J$ and $k = K$, (A3) is formally indeterminate.

b) Stability of the ADI scheme

To demonstrate stability of ('18), assume a periodicity condition in x and Dirichlet conditions in y — however, assuming periodicity in x would make $[\delta_x - \beta(\Delta t/2)\delta_{xx}]$ a singular operator, so its inversion in (18b) is not formally possible. Eliminating $\tilde{\phi}^{n+1}_{j,k}$ in (18b) using (18a) and the inversion of $[\delta_x - (\Delta t/2)\delta_{yy}]$ leads after some rearrangement to

$$(\delta_x - \frac{\Delta t}{2}\beta\delta_{xx})\tilde{\phi}^{n+1} = \left(\delta_x - \frac{\Delta t}{2}\delta_{yy}\right)^{-1}\left[\left(\delta_x + \frac{\Delta t}{2}\delta_{yy}\right)\left(\delta_x + \beta\frac{\Delta t}{2}\delta_{xx}\right)\right]\tilde{\phi}^{n} \tag{A4}$$

Again the coefficient matrices can be simultaneously diagonalized by unitary transformations, and stability depends only on the eigenvalues. In the transformed variables, $\hat{\phi}$

$$\left[(\Delta x)^{-1}\left(1 - e^{-i\theta_j}\right) + \left(\frac{\Delta t}{2}\right)\left(\frac{1}{\Delta x}\right)^2 4\beta \sin^2\left(\frac{\theta_j}{2}\right)\right]\hat{\phi}^{n+1}_{j,k}$$

$$= \left[\frac{(\Delta x)^{-1}\left(1 - e^{-i\theta_j}\right) - \frac{\Delta t}{2}\,4\sin^2\left(\frac{\theta_k}{2}\right)}{(\Delta x)^{-1}\left(1 - e^{-i\theta_j}\right) + \frac{\Delta t}{2}\,4\sin^2\left(\frac{\theta_k}{2}\right)}\right]\left[(\Delta x)^{-1}\left(1 - e^{-i\theta_j}\right) - \frac{\Delta t}{2}\left(\frac{1}{\Delta x}\right)^2 4\beta \sin^2\left(\frac{\theta_j}{2}\right)\right]\hat{\phi}^{n}_{j,k} \tag{A5}$$

For $\sin^2(\theta_j/2) \neq 0$ the left-hand coefficient can be divided out, and one can readily show that a ratio of eigenvalues appear which has the same type of inequality as (A3). Thus for all roots such that $\sin^2(\theta_j/2) > 0$, stability is unconditional. For the singular case, when $\sin(\theta_j/2) = 0$, the system is formally indeterminant.

APPENDIX B

A scheme is considered here that illustrates loss of conservation form by the use of proper conservative spatial differencing but with an improper time linearization. An interesting property of the scheme is that arbitrarily large time steps can be taken without generating the type of instability discussed in Section III.

An implicit, first-order accurate approximation to (21) is given by

$$(1 - E_x^{-1})(\phi_j^{n+1} - \phi_j^n)$$

$$= \frac{-\Delta t}{\Delta x}\left[(1 - \epsilon_j)(\hat{\phi}_{j+1} - \hat{\phi}_{j-1})(E_x^{+1} - 1) + \epsilon_{j-1}(\hat{\phi}_j - \hat{\phi}_{j-2})(1 - E_x^{-1})\right](1 - E_x^{-1})\phi_j^{n+1} \qquad (B1)$$

which uses the notation defined in Section III and where $\hat{\phi}_j = \phi_j^{n+1}$. To avoid solving a nonlinear system at each time level, the first-order accurate approximation $\hat{\phi}_j = \phi_j^n$ is made. With this approximation it can be shown by a flux summation argument that, for (B1) applied to the model data shown in figure 3, the shock speed is

$$\frac{dx_s}{dt} = \frac{\phi_{x_L} + \phi_{x_R}}{1 + \frac{\Delta t}{\Delta x}\left(\phi_{x_L} - \phi_{x_R}\right)} \qquad (B2)$$

whereas the correct shock speed for (21) is

$$\frac{dx_s}{dt} = \phi_{x_L} + \phi_{x_R} \qquad (B3)$$

Thus (B1) satisfies the correct shock conditions only for stationary shocks ($\phi_{x_L} = -\phi_{x_R}$), shocks with zero strength ($\phi_{x_L} = \phi_{x_R}$), or when $\Delta t/\Delta x \to 0$.

An interesting feature of this nonconservative (in time) scheme is that as $\Delta t/\Delta x \to \infty$, the shock speed approaches zero, as shown in figure 17. In fact, $\tau \to (\phi_{x_L} + \phi_{x_R})/(\phi_{x_L} - \phi_{x_R})$ as $\Delta t/\Delta x \to \infty$. Hence, from (33), no instabilities are expected to occur for large Δt, and numerical experiments confirm this. This feature is attractive in applications in which only the steady-state solution is of interest, and using (B1) with the first-order AF scheme does indeed provide a very effective relaxation algorithm.

REFERENCES

1. Landahl, M.: Unsteady Transonic Flow. Pergamon Press, New York, 1961.

2. Beam, R. M.; and Ballhaus, W. F.: in NASA SP-347, 2, 1975.

3. Ballahus, W. F.; Magnus, R.; and Yoshihara, H.: In Unsteady Aerodynamics 2 (R. B. Kinney, ed.) University of Arizona Press, Arizona, 1975.

4. Ballhaus, W. F.; and Lomax, H.: In Lecture Notes in Physics, 35, Springer-Verlag, New York, 1975.

5. Douglas, J., Jr.; and Gunn, J. E.: Numer. Math. 6 (1964), 428.

6. Yanenko, N. N.: The Method of Fractional Steps, Springer-Verlag, New York, 1971.

7. Mitchell, A. R.: Computational Methods in Partial Differential Equations, Wiley, New York, 1969.

8. Beam, R. M.; and Warming, R. F.: (Submitted for publication to J. of Comp. Physics.)

9. Murman, E.: In Proc. AIAA Computational Fluid Dynamics Conf., July, 1973.

10. Caradonna, F. X.; and Isom, M. P.: AIAA Paper No. 75-168, 1975.

11. Marcus, M.: Basic Theorems in Matrix Theory, Nat. Bu. Standards Appl. Math Ser. 57 (1960).

12. Bellman, R.: Introduction to Matrix Analysis, (2nd ed.), McGraw-Hill, New York, 1970.

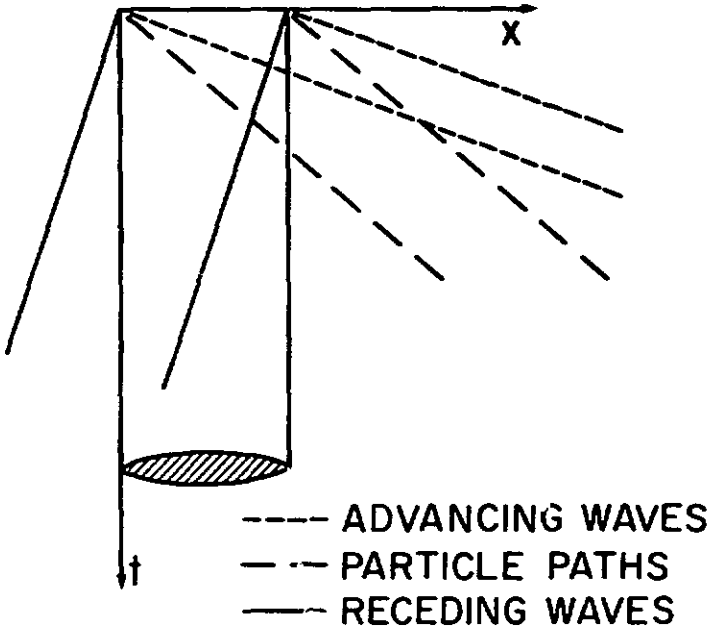

Figure 1a.- Characteristics for the small-disturbance equation (1).

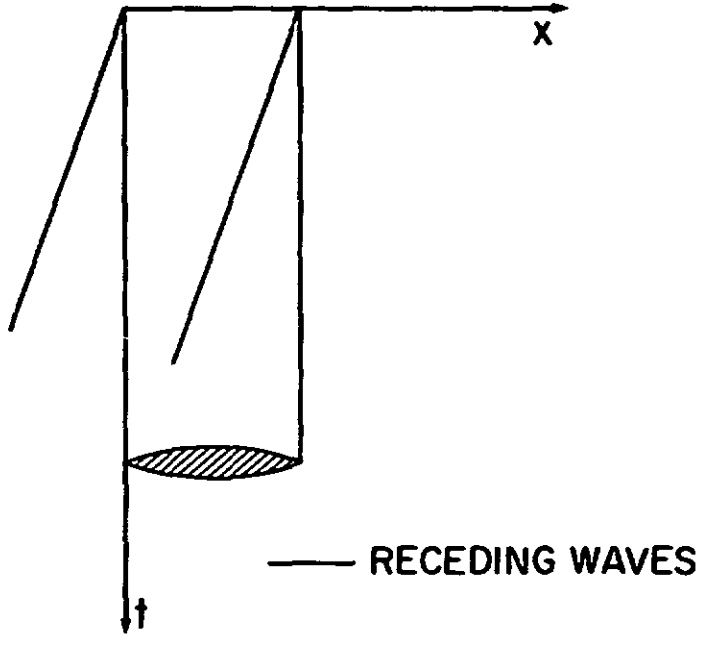

Figure 1b.- Characteristics for the low-frequency approximation (4).

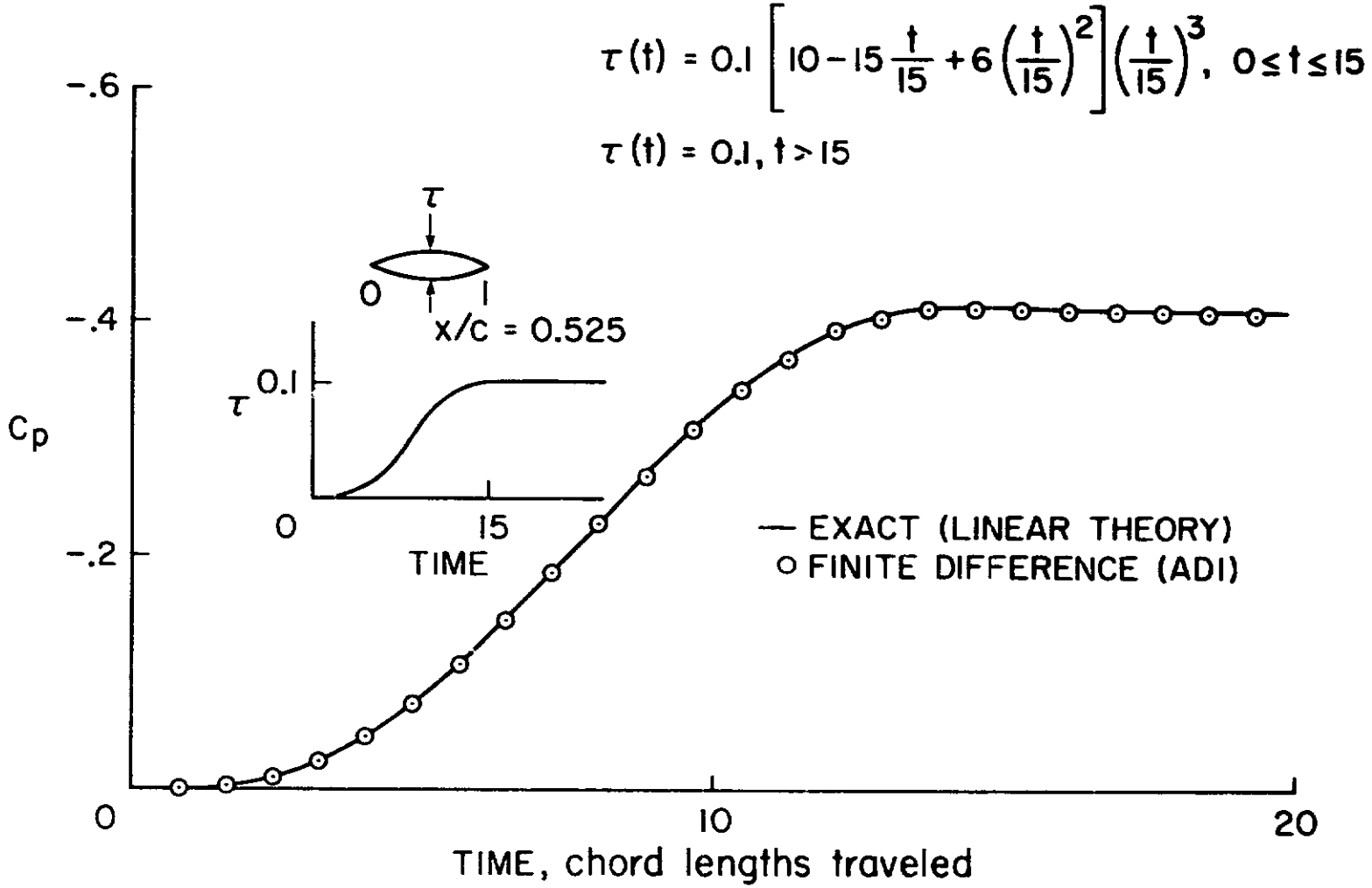

Figure 2.- Midchord pressure coefficients vs time for a thickening parabolic arc airfoil, M = 0.785.

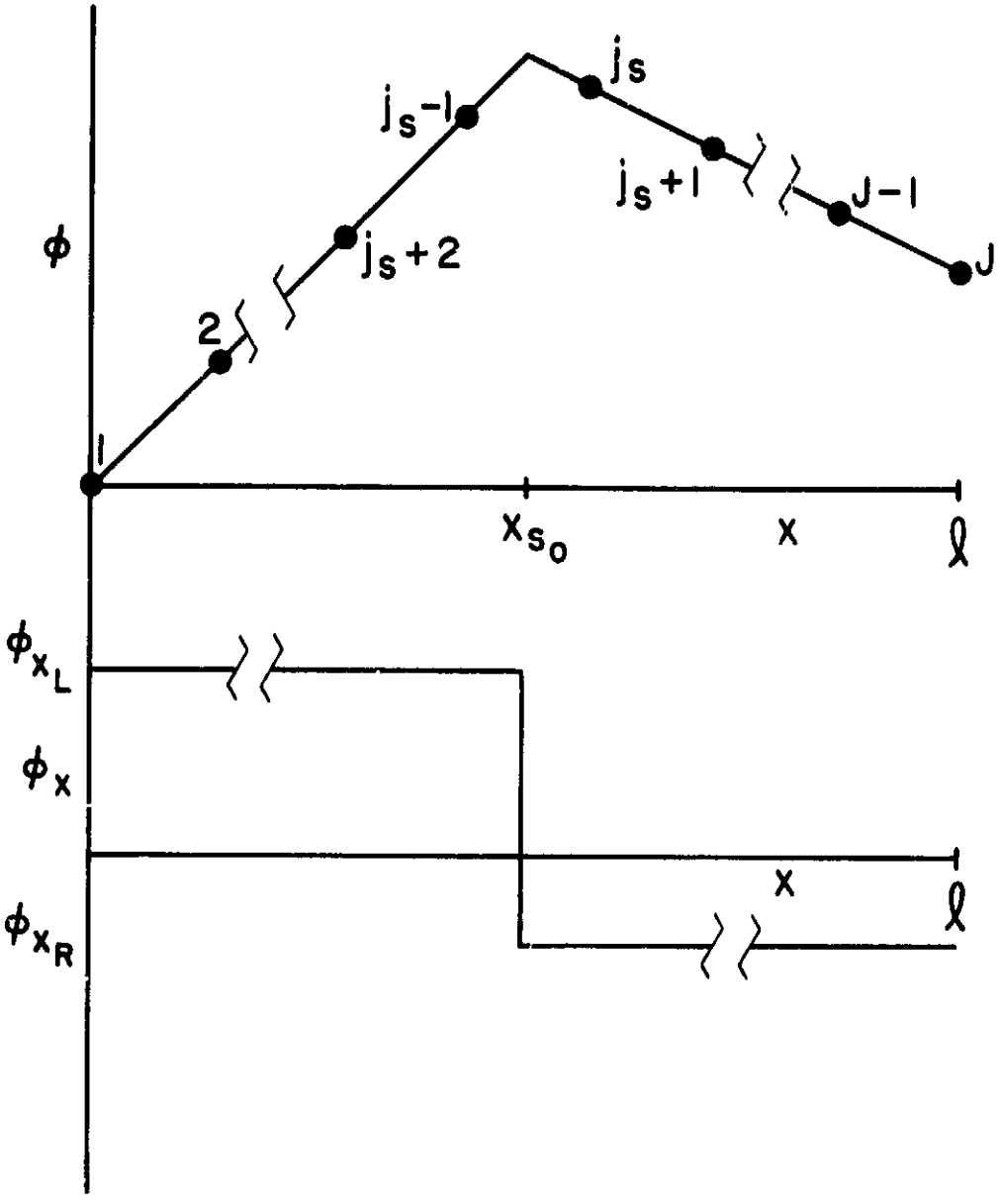

Figure 3.- Sketch of initial data for model one-dimensional problem.

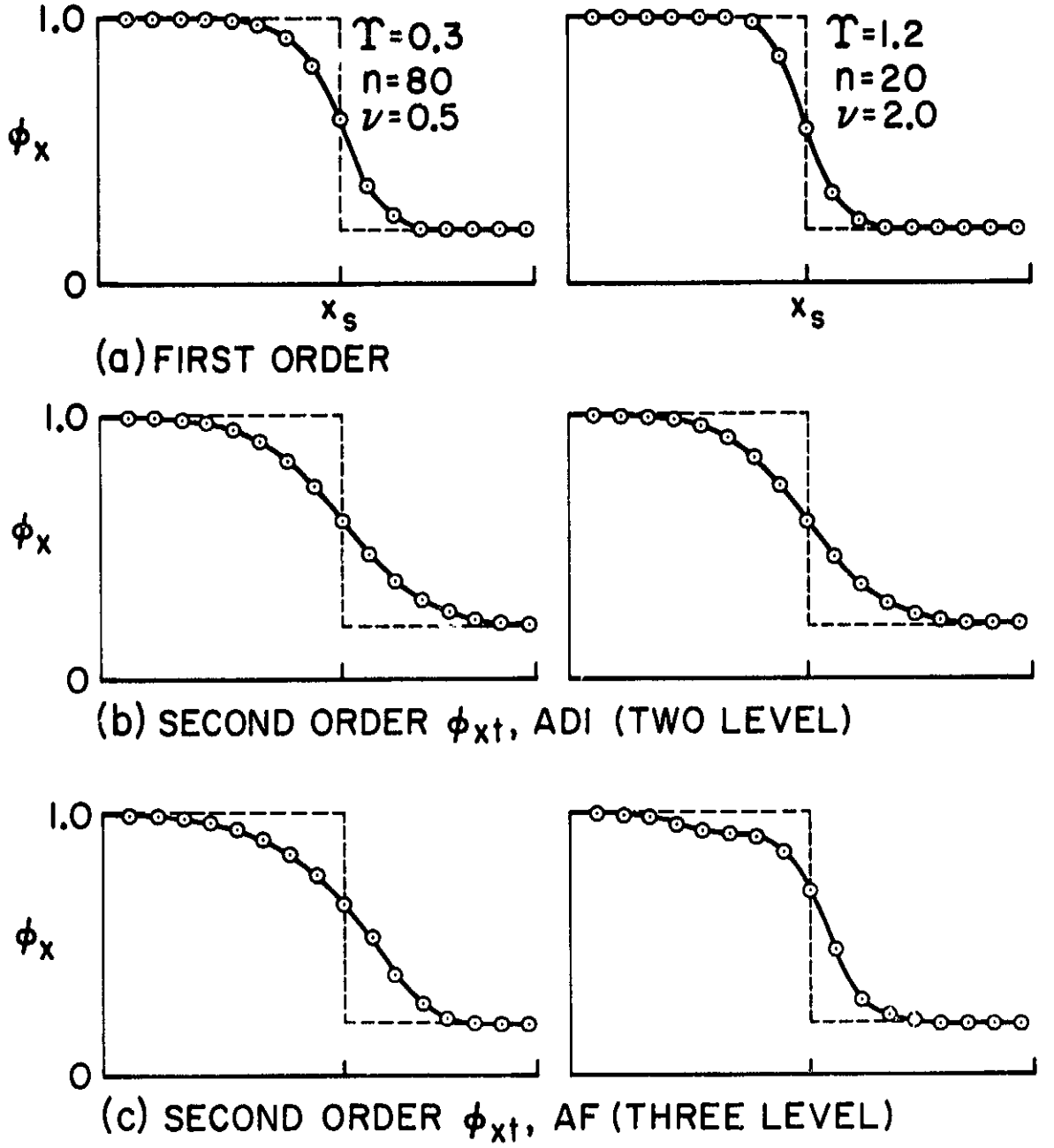

Figure 4.- Shock profiles for supersonic-to-supersonic case.

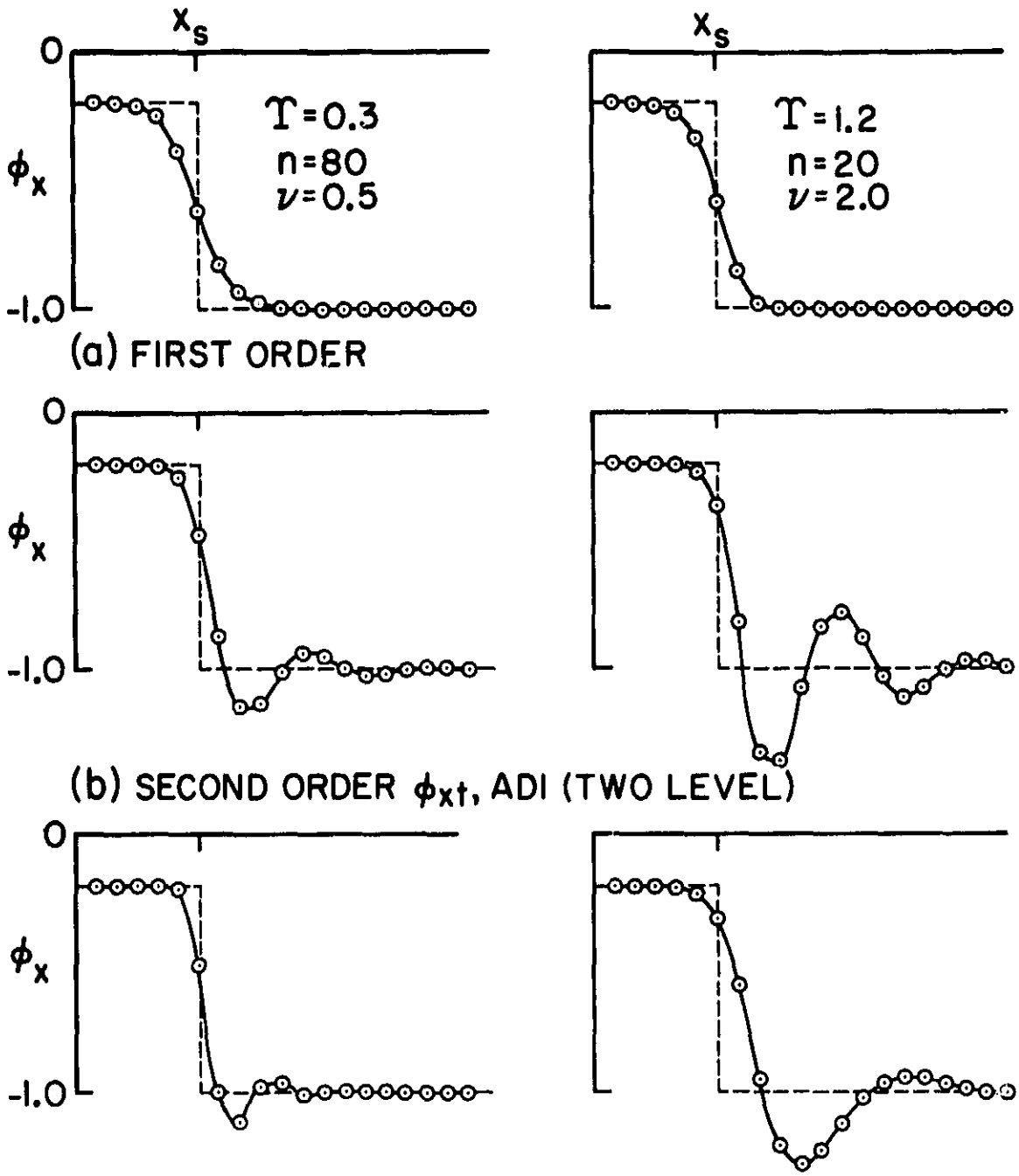

Figure 5.- Shock profiles for subsonic-to-subsonic case.

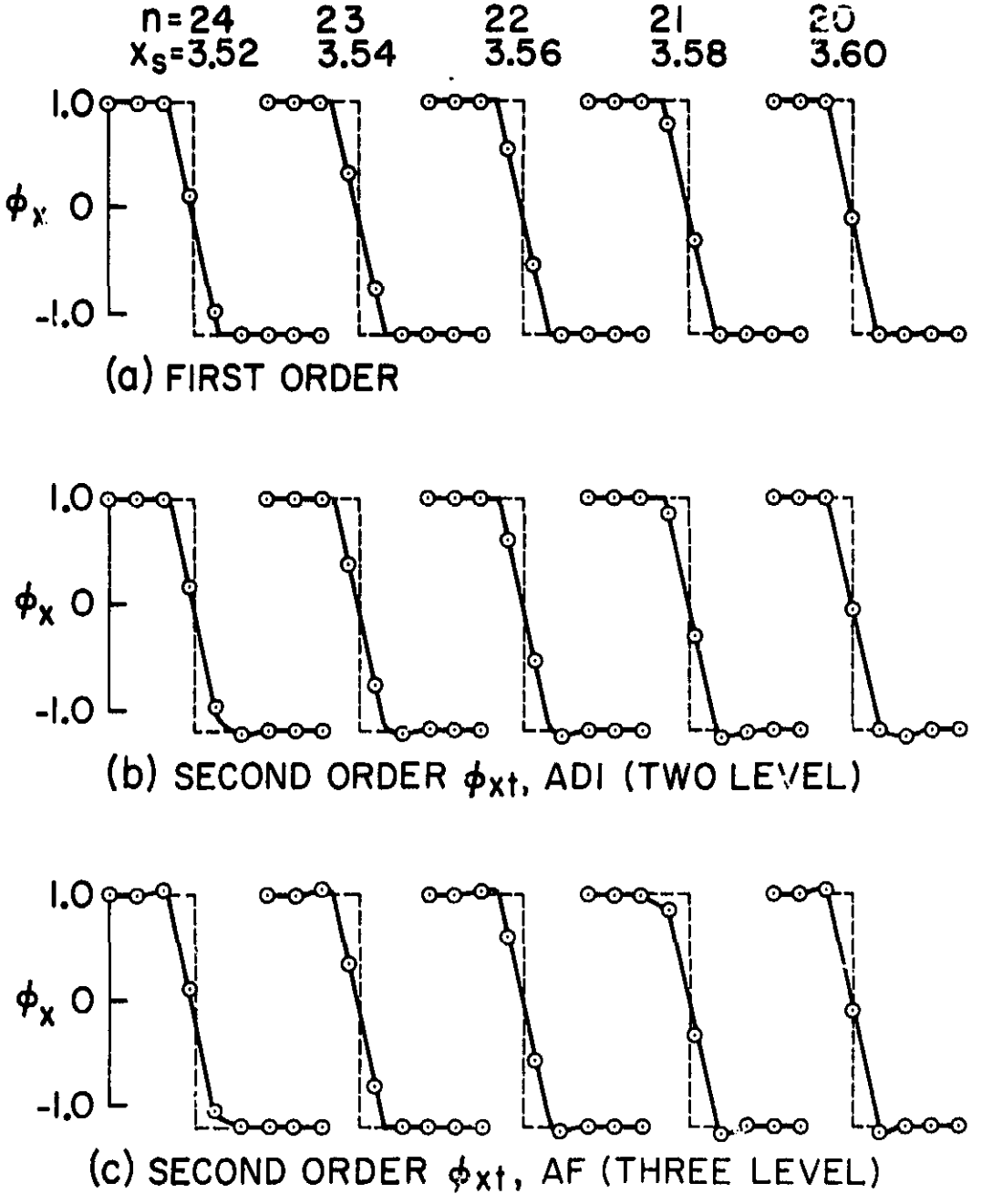

Figure 6.- Shock profiles for upstream-moving, supersonic-to-subsonic case, $T = 0.2$, $\nu = 2.4$.

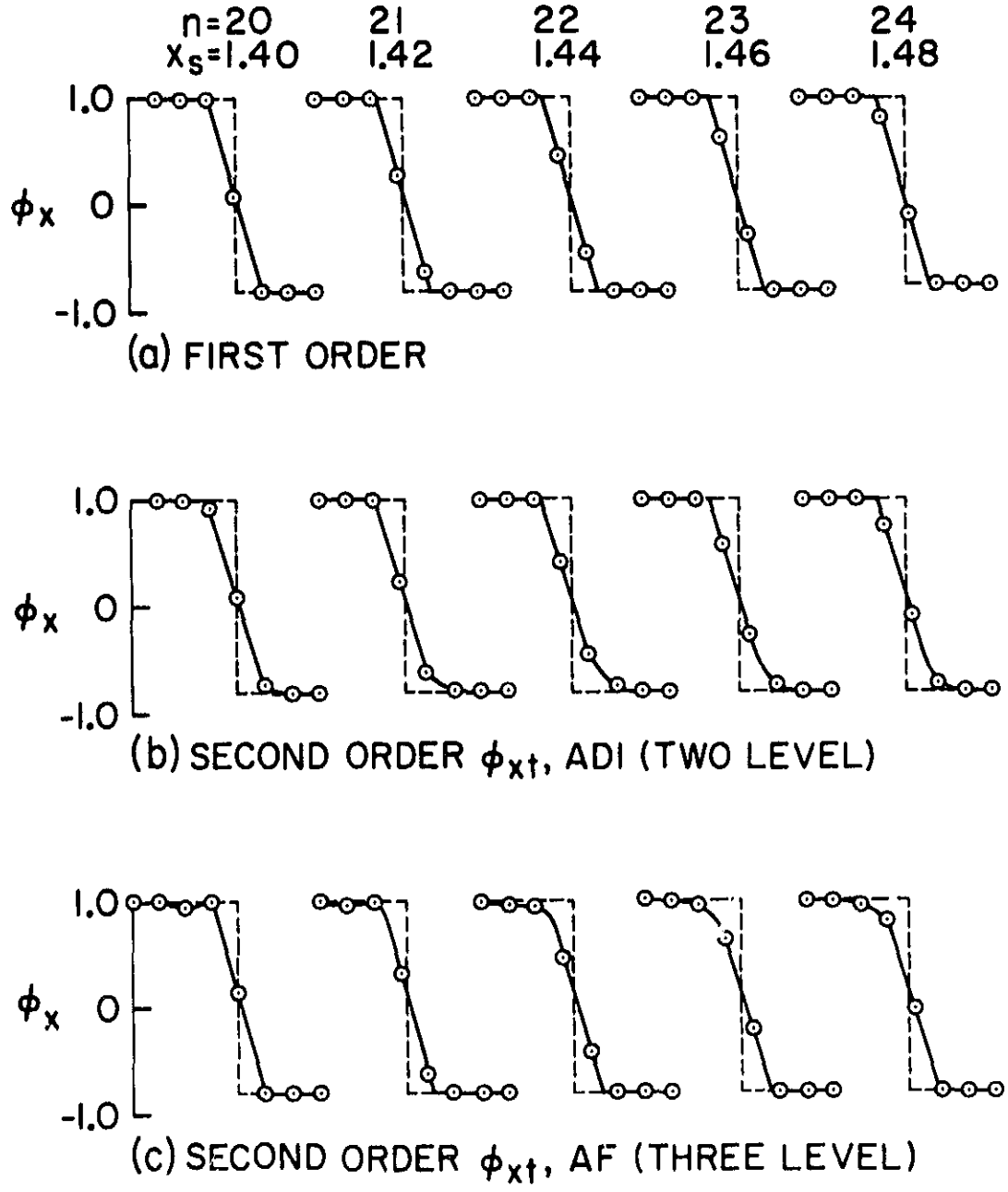

Figure 7.- Shock profiles for downstream-moving, supersonic-to-subsonic case, T = 0.2, ν = 2.0.

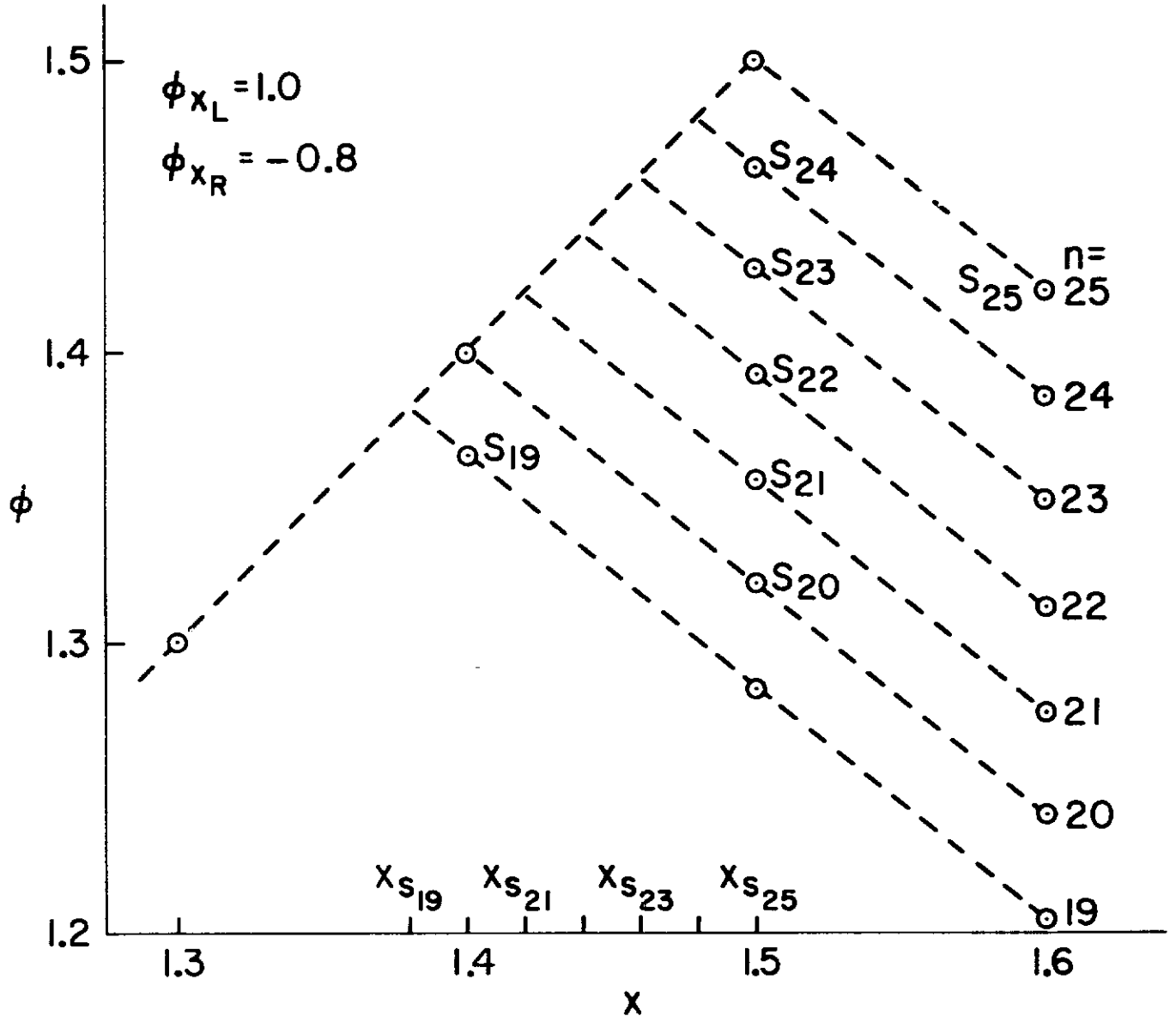

Figure 8.- ϕ vs x for downstream moving, supersonic-to-subsonic case, T = 0.2, ν = 2.0.

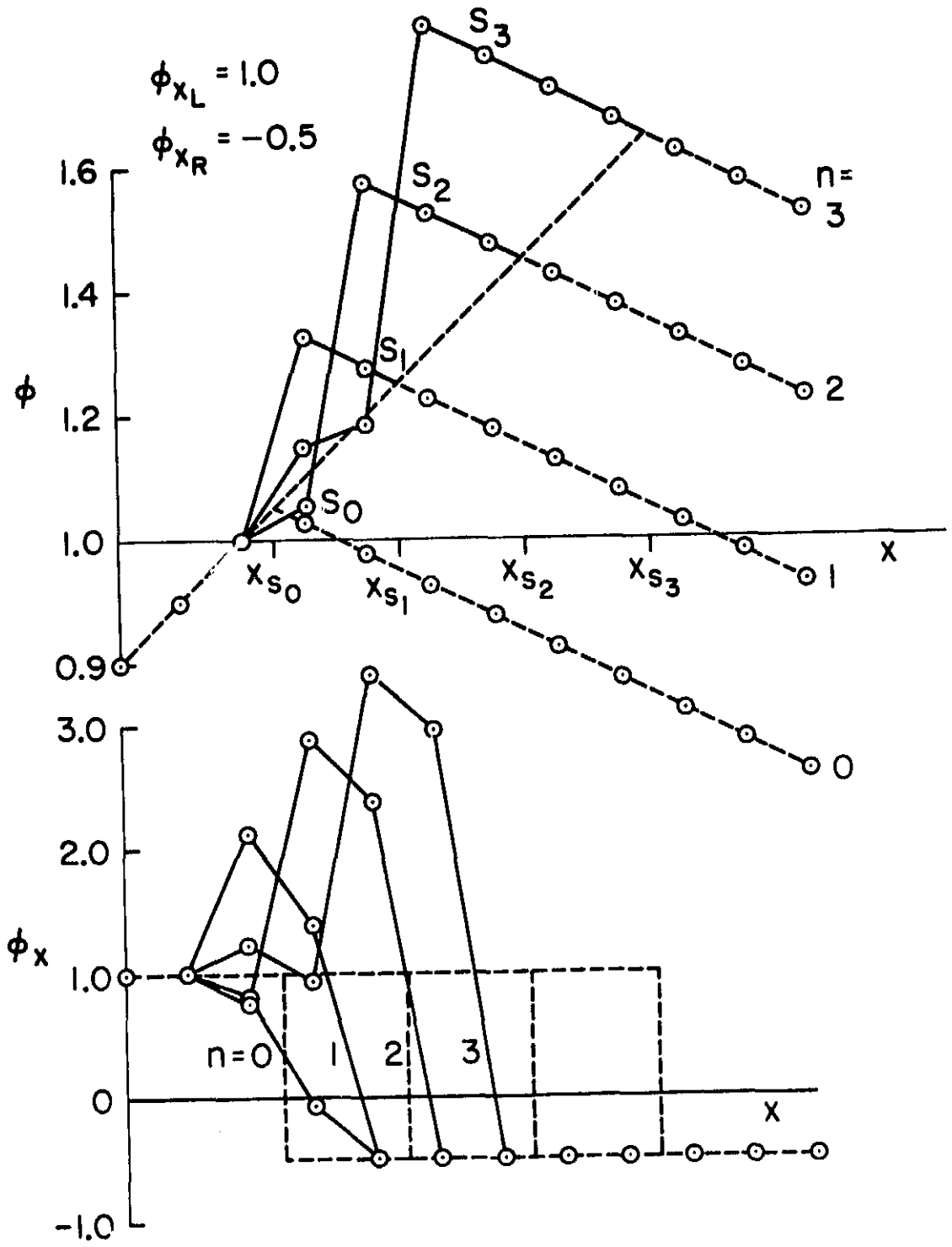

Figure 9.- First-order results for $T = 2.0$, $\nu = 8.0$.

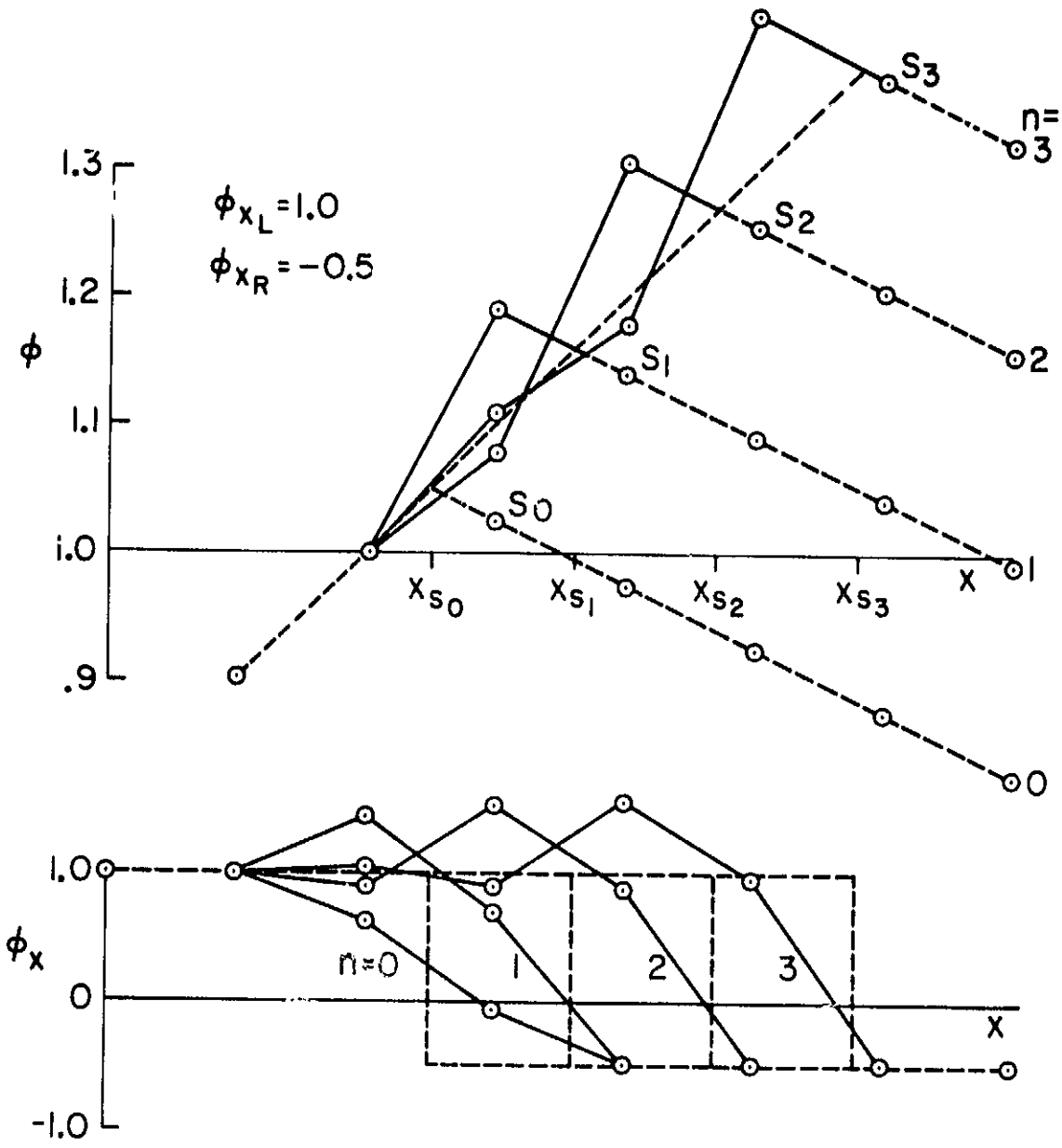

Figure 10.- First-order results for $T = 1.1$, $\nu = 4.4$.

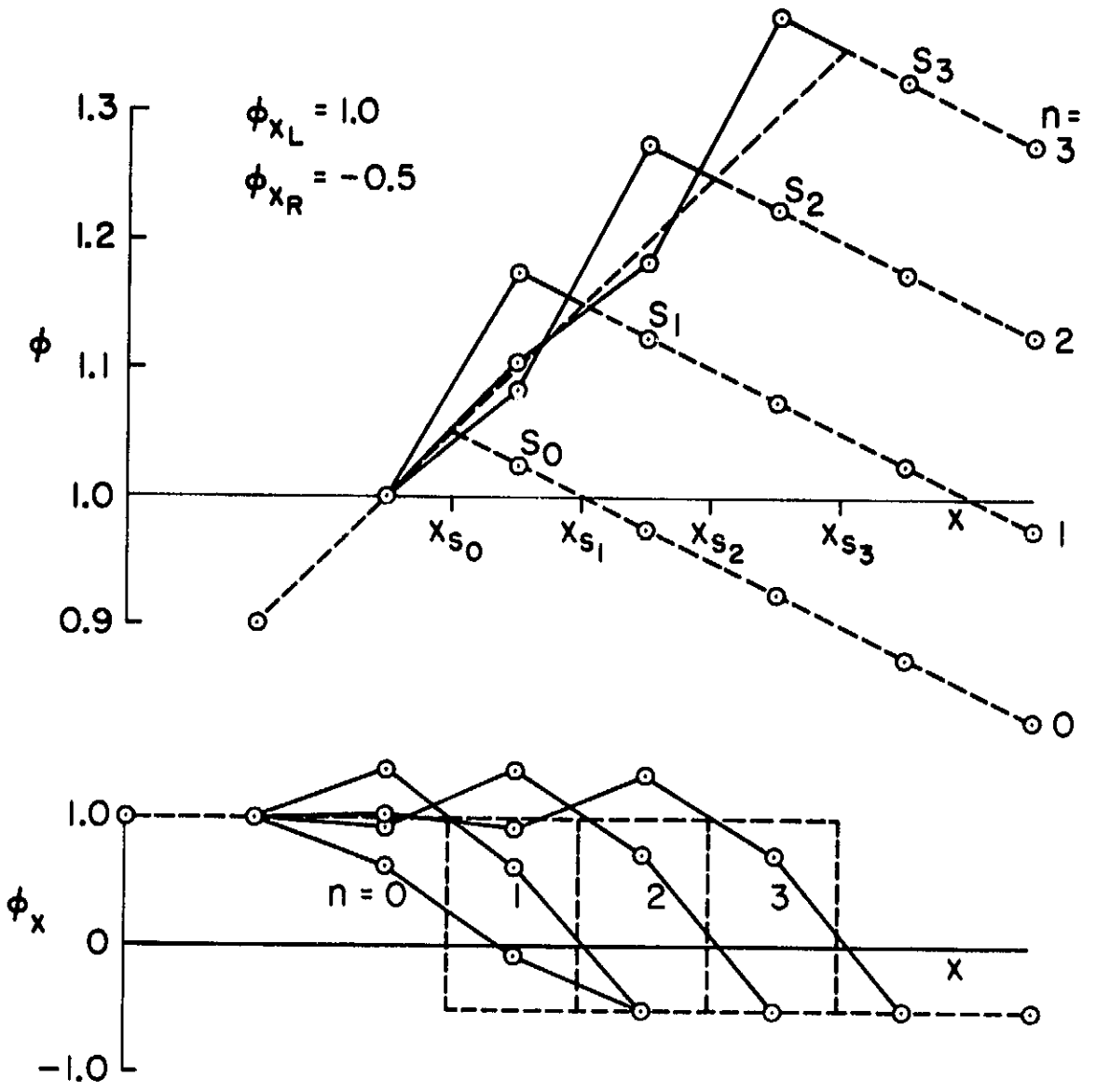

Figure 11.- First-order results for $T = 1.0$, $\nu = 4.0$.

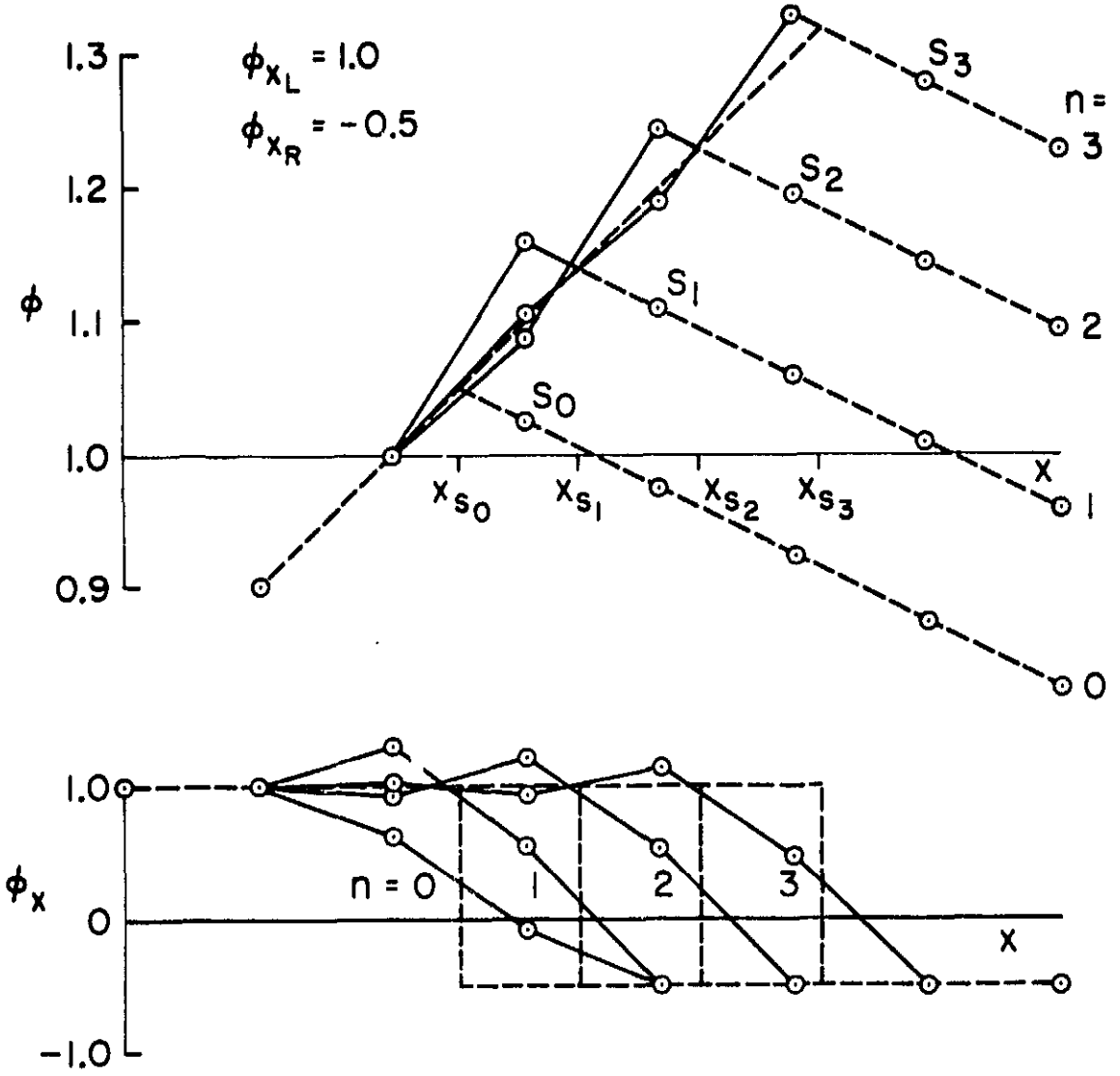

Figure 12.- First-order results for $T = 0.90$, $\nu = 3.6$.

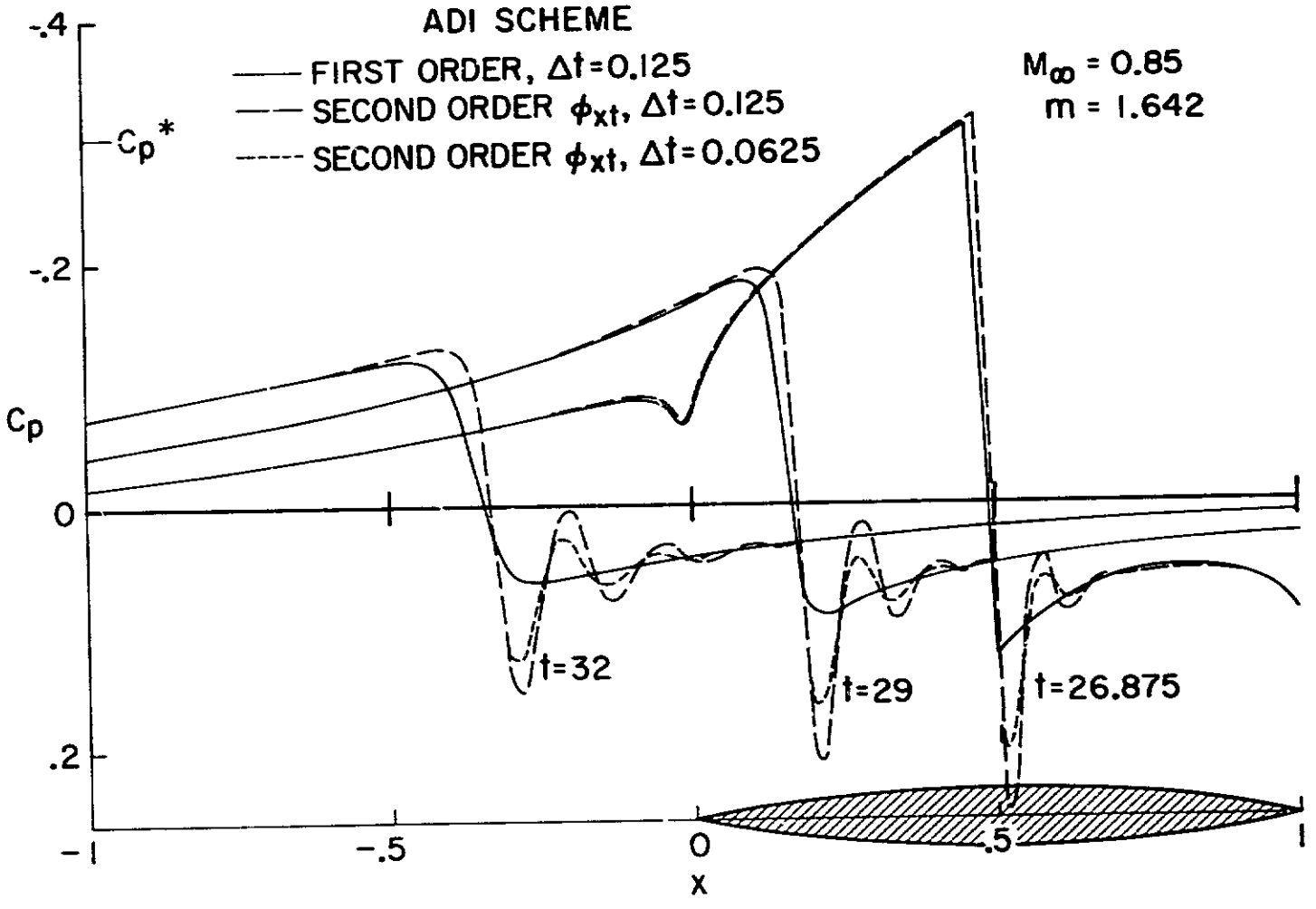

(a) ADI scheme.

Figure 15.- Pressure coefficient for upstream propagation of the shock wave.

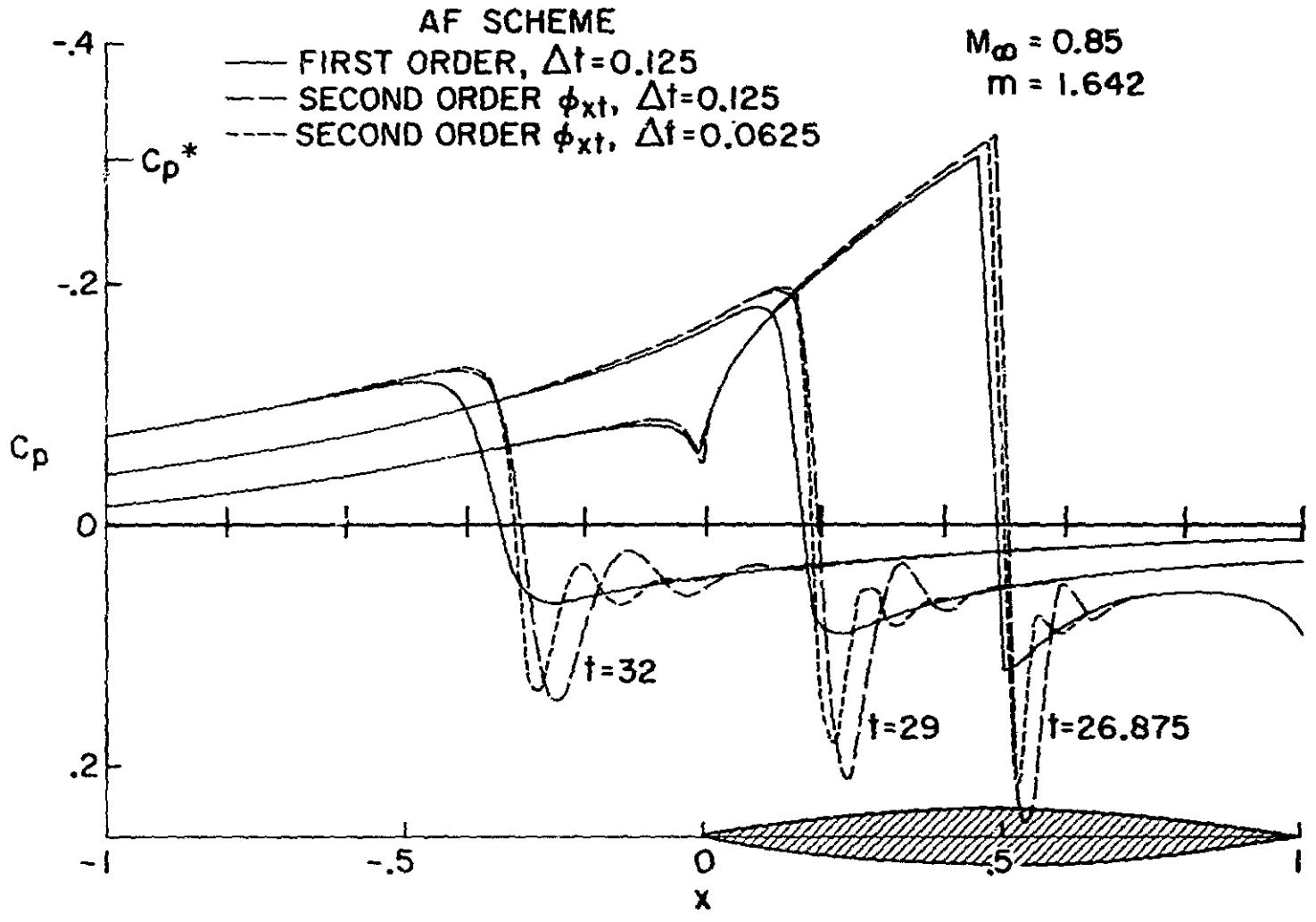

(b) AF scheme.

Figure 15.- Concluded.

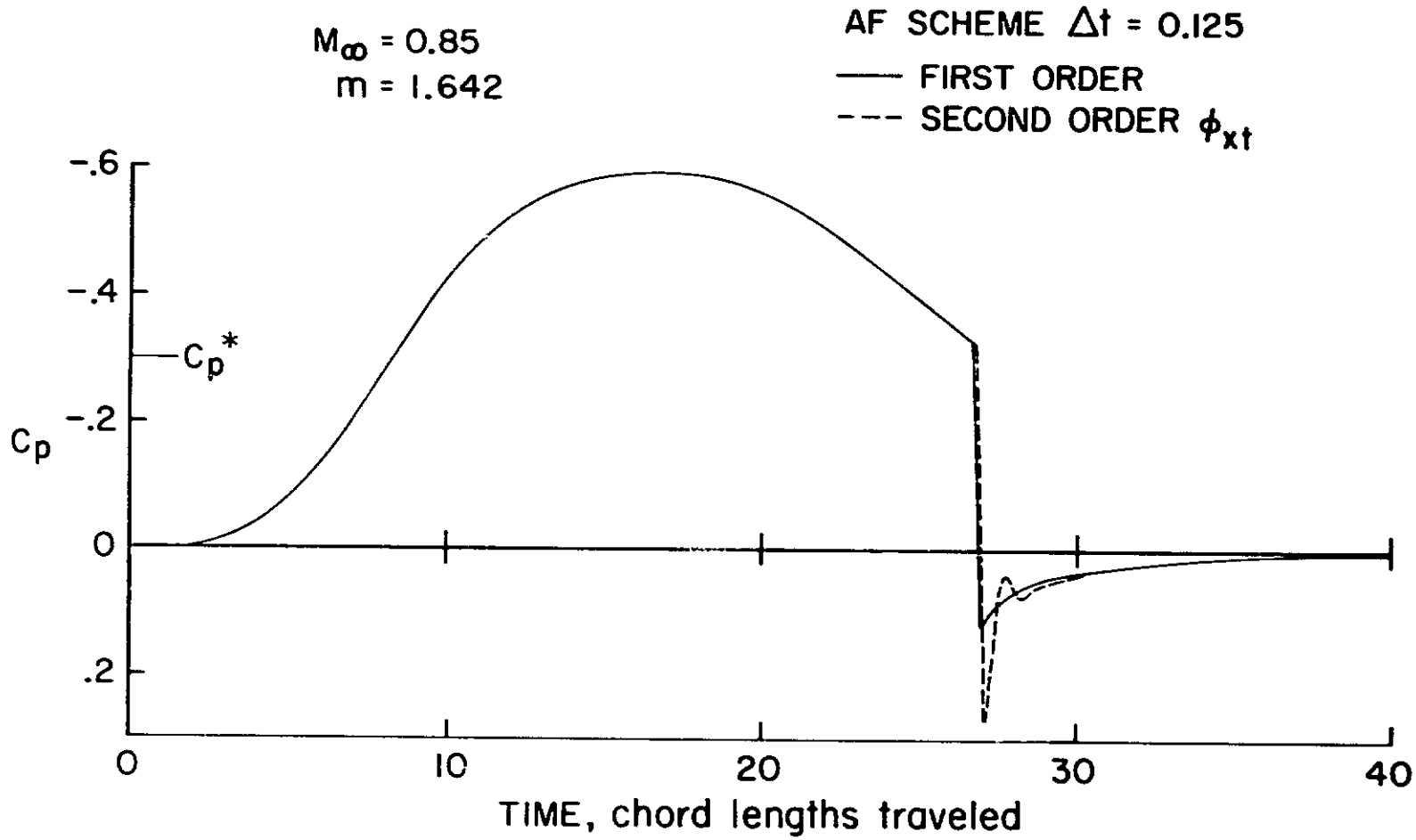

(a) ADI scheme.

Figure 16.- Midchord pressure coefficient vs time.

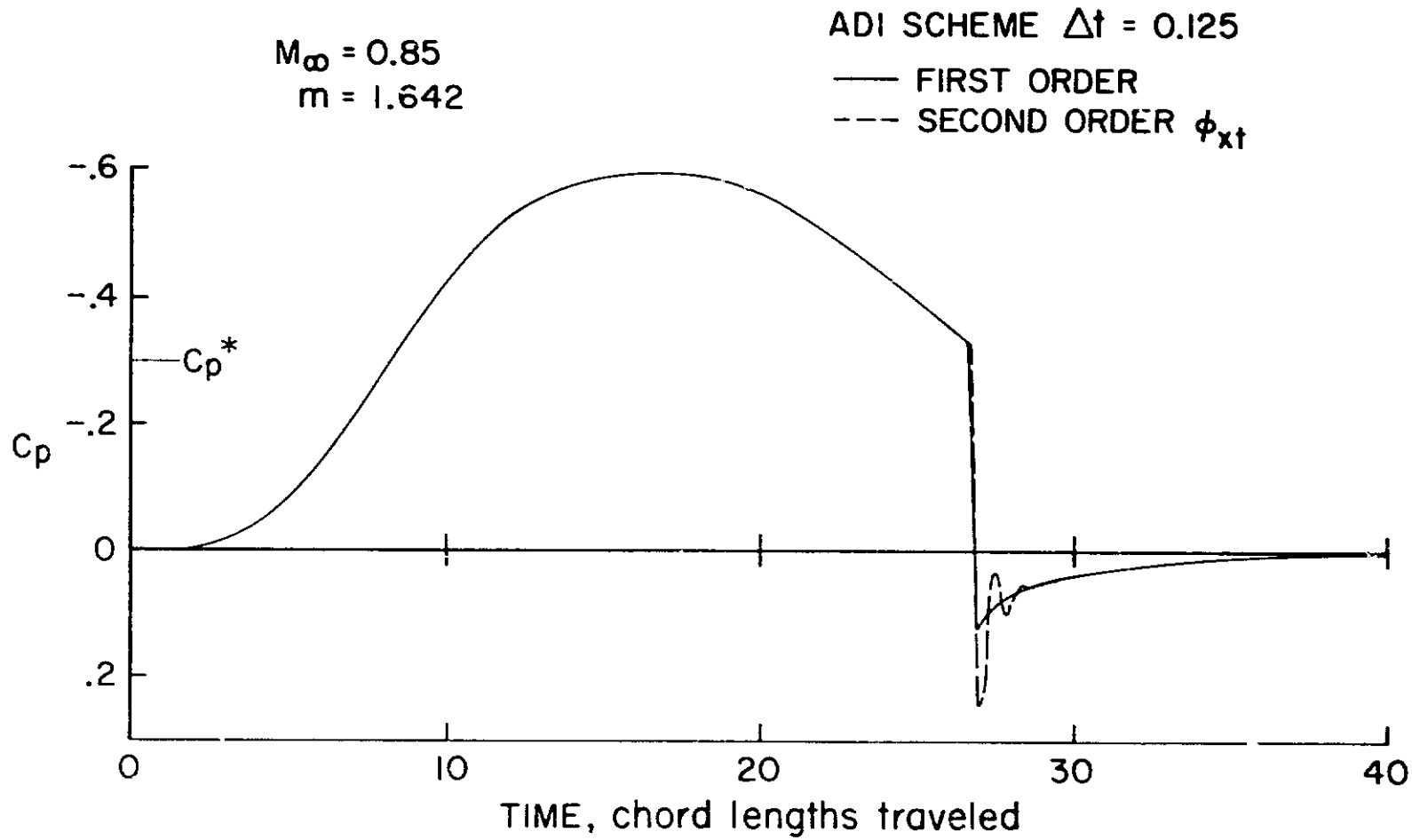

(b) AF scheme.

Figure 16.- Concluded.

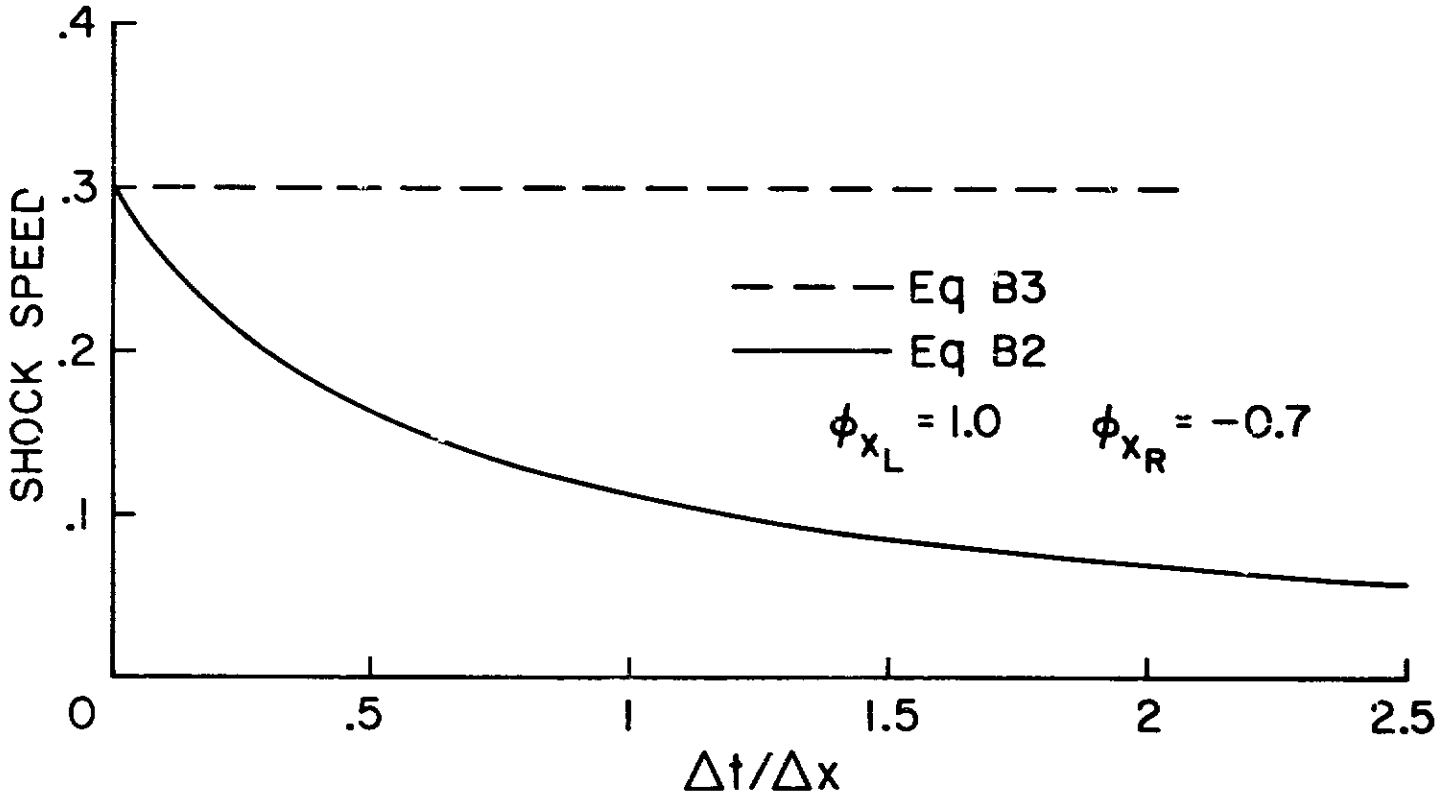

Figure 17.- Shock speed vs $\Delta t/\Delta x$.